Biological, geological and chemical effects of oxygen injection in underground gas storage aquifers in the setting of biomethane deployment

Perla Haddad, Jean Mura, Franck Castéran, Marion Guignard, Magali Ranchou-Peyruse, Pascale Sénéchal, M. Larregieu, M.-P. Isaure, Isabelle Svahn, Peter Moonen, et al.

Biological, Geological and Chemical Effects of Oxygen Injection in Underground Gas Storage Aquifers in the setting of Biomethane Deployment

Perla G. HADDAD[1], Jean MURA[1], Franck CASTERAN[1,2], Marion GUIGNARD[3], Magali RANCHOU-PEYRUSE[1,2,3], Pascale SENECHAL[4], Marie LARREGIEU[3], Marie-Pierre ISAURE[3], Isabelle SVAHN[5], Peter MOONEN[4], Isabelle LE HECHO[2,3], Guilhem HOAREAU[6], Pierre CHIQUET[2,7], Guilhem CAUMETTE[2,7], David DEQUIDT[8], Pierre CEZAC[1,2], Anthony RANCHOU-PEYRUSE[2,3*]

[1] Université de Pau et Pays de l'Adour, E2S UPPA, LaTEP, Pau, France.

[2] Joint Laboratory SEnGA, UPPA-E2S-Teréga, Pau, 64000, Pau, France.

[3] Université de Pau et Pays de l'Adour, E2S UPPA, CNRS, IPREM, Pau, France.

[4] Université de Pau et Pays de l'Adour, E2S UPPA, CNRS, DMEX, Pau, France.

[5] Bordeaux Imaging Center (BIC), CNRS, Université de Bordeaux, Bordeaux, France.

[6] Université de Pau et Pays de l'Adour, E2S UPPA, CNRS, TOTAL, LFCR, Pau, France.

[7] Teréga – Geosciences Department, Pau, France.

[8] STORENGY – Geosciences Department, Bois-Colombes, France.

*Correspondence: anthony.ranchou-peyruse@univ-pau.fr

Phone: +33 540 145 164

Abstract

The last few years have seen the proliferation of anaerobic digestion plants to produce biomethane. Oxygen (O_2) traces added to biogas during the desulfurization process are co-injected in the gas network and can be stored in Underground Gas Storage (UGS). However, there are no data available for the undesirable effects of O_2 on these anoxic environments, especially on deep aquifers. In addition to mineral alteration, O_2 can have an impact on the anaerobic autochthonous microbial life. In our study, the storage conditions of an UGS aquifer were reproduced in a high-pressure reactor and bio-geo-chemical interactions between the aqueous, gas and solid phases were studied. Sulfate was depleted from the liquid phase for three consecutive times during the first 130 days of incubation reproducing the storage conditions (36 °C, 60 bar, methane with 1% CO_2). Sulfate-reducers, such as *Desulfovibrionaceae*, were identified from the high-pressure system. Simulations with PHREEQC were used to determine the thermodynamic equilibrium to confirm any gas consumption. CO_2 quantities decreased in the gas phase, suggesting its use as carbon source by microbial life. Benzene and toluene, hydrocarbons found in traces and known to be biodegradable in storages, were monitored and a decrease of toluene was revealed and associated to the *Peptococcaceae* family. Afterwards, O_2 was added as 1% of the gas phase, corresponding to the maximum quantity found in biomethane after desulfurization process. Re-oxidation of sulfide to sulfate was observed along with the end of sulfate reducing activity and toluene biodegradation and the disappearance of most of the community. H_2 surprisingly appeared and accumulated as soon as hydrogenotrophic sulfate-reducers decreased. H_2 would be produced *via* the necromass fermentation accomplished by microorganisms able to resist the oxic conditions of $4.42 \cdot 10^{-4}$ mol.Kgw^{-1} of O_2. The solid phase composed essentially of quartz, presented no remarkable changes.

Keywords: deep aquifers, biomethane, oxygen, deep subsurface, high pressure, UGS, geological storage

1. Introduction

Oxygen (O_2) can be injected in deep underground for many purposes. Its ability to promote aerobic microbial metabolism is a key factor to achieve the endpoint in multiple current practices especially during the application of enhanced oil recovery techniques on oil reservoir (Cai et al., 2015; Liu et al., 2018; Pannekens et al., 2019) and the bio-remediation of groundwater (EPA, 2017; Lien et al., 2016; Trulli et al., 2016). However, despite its aforementioned beneficial applications, the presence of oxygen can be deleterious during other procedures such as Carbon Capture and Storage (CCS) (Morgan et al., 2017; Wei et al., 2015), compressed air energy storage (CAES) (Guo et al., 2021; Kushnir et al., 2012) and underground natural gas storage (UGS). Many studies have been undergone in the context of CCS storage in order to define the effect of carbon dioxide, but also the effect of oxygen injected as an impurity on the geological formations. Similarly, the deep underground storage of biomethane can also involve co-injection of O_2. Indeed, O_2 is added to the biomethane during sulfide reoxidation at the outlet of the anaerobic digestion plant. Depending on the initial sulfide quantity, the proportion of O_2 may attain 1.5 % of the final gas mixture (Barik et al., 2013). For underground gas storage, France sets a maximal O_2 proportion of 100 ppm, whereas Germany sets a maximal of 10 ppm.

Biomethane is an attractive alternative to fossil fuels particularly because biogas produced from biomass, such as green waste and sludge from wastewater, prevents re-circulating carbon from oil, natural gas and coal. With a reported production of 1.2 billion m^3 in 2015, Europe is the world's leading biomethane producer. The lead application of the produced biomethane consists of its use as vehicle fuel or its injection into the natural gas grid (Scarlat et al., 2018). With the fluctuating and unpredictable demand throughout the year, biomethane storage is recently gaining an increasing interest. Due to their large storage capacity and their ability to preserve gas under pressure, deep aquifers emerge as attractive underground storage

systems. Deep Underground Gas Storages (UGS) such as deep aquifers, are known for being anoxic environments that form large ecosystems and harbor a much-diverse anaerobic microbial life (Magnabosco et al., 2018). The biodegradation of hydrocarbons was notably studied in this setting, especially the anaerobic degradation of BTEX (Benzene, Toluene, Ethylbenzene and Xylenes isomers) by autochthonous microorganisms in these ecosystems (Aüllo et al., 2016; Bombach et al., 2010; Ranchou-Peyruse et al., 2017). Sulfate-reducing bacteria (SRB) are particularly known to be active and to be key players in such anoxic environments (Berlendis et al., 2010; Bombach et al., 2010; Detmers et al., 2004; Fry et al., 1997; Itävaara et al., 2011; Ranchou-Peyruse et al., 2019). Part of the O_2 co-injected with the biomethane during its storage can solubilize into the formation water leading to alterations of the preexisting thermodynamic equilibrium, which can result in drastic modifications in the microbial communities and depletion of strictly anoxic micro-organisms. O_2 may also cause mineral oxidation of the reservoir rock (Guo et al., 2021; Jung et al., 2013; Kushnir et al., 2012; Lu et al., 2016; Vu et al., 2018). For instance, the oxidation of pyrite (FeS_2) was observed during CAES in different studies (Guo et al., 2021; Kushnir et al., 2012) and during CCS (Jung et al., 2013; Shao et al., 2014). This alteration can cause a variation in the reservoir's porosity and permeability especially if large amounts of redox-sensitive minerals were present (Lu et al., 2016). Dissolution of rocks, mineral precipitations and corrosion of well materials were shown as possible (Zettlitzer et al., 2010; Wang et al., 2011). Variation in the aqueous phase composition resulting from mineral dissolution can impact the thermodynamic equilibrium. Identifying this equilibrium is important to determine the material balance and to estimate any production or consumption of gas such as carbon dioxide consumption by the microbial life as a carbon source or oxygen consumption due to chemical reactions. However, experimental solubility data corresponding to our aqueous and gas compositions under aquifer's conditions are very limited. The studied conditions of the

system were a temperature of 36 °C and a total pressure of 60 bar, similar to the aquifer's real storage conditions. Even though many CCS studies targeted storage effects on the site, multiple uncertainties remain regarding the effects of impurities namely O_2 during biomethane storage in natural gas reservoirs such as aquifers. In order to elucidate more answers on this topic, a multi-disciplinary study is undergone and, to our knowledge, this is one of few studies involving the reproduction of the aquifer's *in-situ* conditions in a reactor using solid, liquid and microbial underground samples. During this study, the aqueous and gas compositions were followed up regularly *via* chromatography techniques. Samples from the aqueous phase were recovered under anoxic conditions for microbial studies. Afterwards, O_2 was injected at 1% of the gas mixture, corresponding to the maximum quantity found in biomethane. Before and in the end of the experiment, the solid phase composed of a reservoir rock sample undergone mineral analyses. The subsequent bio-geo-chemical interactions between the gas mixture, reservoir rock, formation water and harbored microbial life were determined under temperature and pressure of a selected aquifer UGS.

2. Materials and methods

2.1- Site description and formation water characteristics.

The studied reservoir is a UGS in the South Aquitaine sedimentary basin (582 m depth), in Southwest France used for natural gas storage since 1981. The well that was selected for this study is the closest to the gas bubble (about 250 m) and has already been identified in previous studies with the code name Ab_L_1 (Ranchou-Peyruse et al., 2019). Thus, sampled water is the most exposed for gases interactions due to its proximity to the gas bubble. Some of the physicochemical characteristics of the formation water (LCE-SOBEGI Laboratory, Lacq, France) and its overall composition were summarized in Table 1. Formation water

(0.634 L) was recovered from the well under pressure (January 2019) with a downhole sampler, equipped with a PDS Sampler (Leutert Bottom Hole Positive Displacement Sampler) (Kampman et al., 2014). Wellhead water samples were also recovered. Samples were stored at 4°C until use. Wellhead samples were filter-sterilized at 0.1 µm (PES 47 mm membranes, 0.1 µm, Sartorius) while maintaining anoxic conditions: 0.854 L of these samples was added to the formation water (0.634 L) to increase the volume, a month before the injection into the high-pressure reactor. A volume of 0.1 L was taken from the final mixture for a microbial diversity study, whereas the rest (1.39 L) was injected into the reactor.

The reservoir rock was composed of infra-molassic sands, with a porosity varying between 25 and 35 % (Ranchou-Peyruse et al., 2019). The rock samples were composed of cuttings collected by TEREGA from a drilling carried out near the studied site. X-ray diffraction analysis applied on the solid sample before the experiment showed that the solid phase was mainly composed of quartz with minor calcite content (Figure S1). Iron sulfides (pyrite and marcasite), iron oxi-hydroxides (maghemite and hematite) and clay minerals were also identified as trace minerals.

2.2- High-pressure reactor.

The apparatus was composed of an experimental cell presented in Figure 1. The autoclave was made of Hastelloy C-276 in order to prevent any corrosion problems. A basket held the solid phase and was composed of a metallic disc with pores of less than 10 µm in order to prevent particles from falling to the bottom of the reactor without interfering with the movement of microorganisms. The operating pressure and temperature can go up to 150 bar and 150 °C respectively. A safety valve of 150 bar connected to a pressure compensation chamber protected the overall system. An insulating coating with heating resistors heated the autoclave. Two thermocouples permitted monitoring of the liquid and gas phase temperatures with a precision of ± 1 °C. A double jacket was used to maintain the temperature of the

experimental cell. The cell pressure was monitored by the Keller PA(A)-33X pressure gauge with a precision of 0.3 bar. In order to maintain a constant pressure throughout the experiment, a mobile piston was placed into the reactor. A 1L capacity pump allowed the piston to move upwards in order to increase the cell pressure and downwards to decrease it. The pump can operate at a maximum pressure of 150 bar and was monitored by a pressure gauge with a precision of 0.05 %. A flow rate of up to 220 mL/min can be imposed with a precision of 0.1 % of the set point. The overall autoclave volume was 5.41 L with an available volume of 4.2 L when the piston was at its lowest level. The solid basket had a volume of 0.8 L. The system was mixed using a stirring shaft operated by a variable speed motor with a maximum stirring speed of 500 rpm. A Rushton turbine was used for the liquid phase and a double disc stirrer with four vertical blades for the gas phase. The composition of the gas mixture injected at the beginning of the biotic experiment was methane, 1 % of carbon dioxide, 7.95 ppm of benzene and 3.57 ppm of toluene. The oxygen added to simulate biomethane injection had a purity of >99.995% (CAS: 7782-55-7).

The experiment ran over 180 days. Initially, a volume of 1.39 L of aqueous phase was injected in the reactor and $4.57 \pm 2.2 \cdot 10^{-1}$ mol of gas mixture. The system liquid-gas-solid-biomass was under development for 130 days under a total pressure of 60 bar and a temperature of 36 °C. The oxygen injection (1 % of 60 bar) occurred at day 131. The Figure 2 presents the analysis undergone through the experiment at different timings.

2.3- Abiotic experiment

A preliminary abiotic experiment was initially undergone in order to detect the liquid-solid interactions before adding the microbial life to the system. 500 mL of distilled water were mixed with 100 mL of sand reservoir in a sealed 1L bottle that was subsequently flushed with N_2 gas at atmospheric pressure. The composition of the aqueous phase was followed in order to detect compounds dissolution from the solid into the liquid phase.

177 *2.4- Analytical analyses.*

178 The liquid phase was analyzed using an ionic chromatography with a variable wavelength
179 detector from ThermoFisher Scientific (Dionex Integrion HPIC). The column IonPac AS28-
180 Fast-4µm (4x150 mm) was used with the AG28-4µm (4x30 mm) guard-column for anion
181 detection, particularly fluoride, chloride, sulfate, acetate, carbonate/bicarbonate and sulfide.
182 The cations were quantified with the Dionex Easion System (ThermoFisher Scientific). The
183 column IC Dionex IonPac CS12A (4x250 mm) was used with the guard-column CG12A
184 (4x50 mm) for sodium, potassium, magnesium and calcium. A liquid sample was taken from
185 the liquid output using a syringe and stored in a flask that was sealed with rubber. Air was
186 immediately extracted from the flask using N_2 gas flush. The sample (1 mL) was directly
187 injected into the instrument. The analyses were performed in triplicate. The supposed
188 measurement uncertainty on both techniques was ± 5%.

189 The gas phase composition was monitored by a gas chromatography in line with a micro
190 thermal conductivity detector (GC-µTCD; Micro GC Fusion; Chemlys; France). The
191 'Molsieve 5A' column was used with helium as a carrier gas for quantification of methane,
192 hydrogen, oxygen and nitrogen. The column 'Plot Q' was used with argon as carrier gas for
193 quantification of carbon dioxide and hydrogen sulfide. The instrument was connected to the
194 reactor's valve. Once open, the sample traversed a pressure compensation tube to reach the
195 piston where it attained the atmospheric pressure and it undergone analysis at that moment.
196 All measures were obtained after three analyses, and the uncertainty was ± 2 %. The obtained
197 results were used to calculate the quantity of each component in the gas phase. The non-ideal
198 gas equation was used to calculate the total number of moles in the autoclave at the moment
199 of analysis. The selected compressibility factor was 0.9 (calculated with PHREEQC using
200 phreeqc.dat as database).

The identification and quantification of benzene and toluene in the liquid and gas phases were performed using a ThermoFisher Scientific gas chromatograph coupled with a quadrupole mass spectrometer (GC-MS) (ISQ QD Single Quadrupole MS - Trace 1310). Preconcentration of benzene and toluene was performed by SPME with a polydimethylsiloxane/carboxene (PDMS/CAR) fiber and the chromatographic separation was performed by a DB-624 column (Agilent). For each sample, two 10 mL water samples were taken and stored at 4°C. Prior to the analysis, 90 µL of the 0.5 ppm 1,2,4-trimethylbenzene internal standard were added to each 6.9 g sample. Gas samples were collected using a needle sampling system controlled by a manometer (1bar/vial). Quantification was performed with methane as reference gas containing 10 mol-ppm of benzene and toluene.

2.5- Treatment of the solid phase.

Before the experiment, the reservoir rock was rinsed with isopropanol followed by water in order to eliminate potential hydrocarbons and salts such as calcium chloride used during the drilling operation. After rinsing, the solid sample was dried and sterilized overnight in the oven at 90°C. A sample of 450 mL of the solid phase was placed in the basket inside the high-pressure reactor. Capillaries used for X-ray tomography were also filled with the solid phase and placed in the basket.

Once the reactor closed, a volume of 60 mL of demineralized water was injected and a flush of N_2 gas was applied. The autoclave was heated to 100 °C during 24h, water vapor was evacuated through the tubes and valves for sterilization. Afterwards the reactor was cooled down, heated to the desired temperature of 36 °C and the water phase (with autochthonous microorganisms) was injected.

After 180 days of experiment at 36 °C and 60 bar, the remaining liquid phase was removed but maintained in sterile and anoxic conditions and was kept at 4°C awaiting further analysis.

225 Afterwards, the solid basket was quickly and carefully removed from the reactor and stored in
226 a sealed anaerobic jar with anaerobiosis generator and indicator pockets (Dutscher Ref
227 0260001) before being transported to an anaerobic glove box.

228 *2.6- Thermodynamic modelling.*

229 The thermodynamic equilibrium at different times of the experiment was calculated using
230 PHREEQC thermodynamic software (Parkhurst and Appelo, 1999). This software allows a
231 comprehensive introduction of dissolved species, solid and gaseous phases and the
232 corresponding chemical reactions. The thermodynamic data were obtained from 'Phreeqc'
233 database without any optimization or modification. Phreeqc.dat uses the extended Debye-
234 Hückel law for activity coefficients and the Redlich-type equation of state for the gas phase.
235 Steady state was assumed for all calculations. All the gas species were considered, but redox
236 reactions of methane and nitrogen were neglected. Water evaporation was considered. Sulfate
237 reduction reaction was not considered in the anoxic part of the experiment. Phreeqc was
238 mainly used to calculate gas solubilities in absence of reactions, thus interactions with the
239 solid phase were not considered. The calculations took into account the different water
240 injections occurring during the experiment and the quantity of gas sampled during the
241 chromatography analysis.

242 *2.7- Cell culture media, strains isolation and brief characterization.*

243 Different synthetic culture media were prepared for the assessment of the microorganisms
244 developed in the reactor just before O_2 addition to the system. In order to prepare these media,
245 a mineral base mimicking the formation water composition was prepared (per liter) by adding
246 0.0002g NH_4Cl; 0.01g KCl; 0.13g $CaCl_2 \cdot 2H_2O$, 0.023g $MgCl_2 \cdot 6H_2O$ and 0.015g K_2HPO_4, 10
247 ml of trace elements solution (SL12; (Eichler and Pfennig, 1986)) and 0.5 mL of selenite
248 tungstate solution (Widdel and Bak, 1992). One gram of cysteine as reducing agent and 1 mL

249 resazurine (0.1% solution, w/v) as redox indicator were supplemented. Depending on the
250 targeted metabolic groups, other compounds were also added. For fermentative bacteria, 10g
251 yeast extract; 2.5g glucose; 15g casein peptone were added whereas for sulfate-reducers,
252 0.82g sodium acetate; 0.5g yeast extract; 0.68g sodium formate; 1.1g sodium pyruvate; 2.84g
253 sodium sulfate were added. Media were autoclaved at 110°C for 30 minutes and then cooled
254 down at room temperature under a stream of N_2. At room temperature, 0.2g of $NaHCO_3$
255 prepared in anoxic conditions and autoclaved separately from the medium was added to each
256 culture medium. Five milliliters of filtered anoxic V10 vitamins solution (Pfennig et al., 1981)
257 were added. Media were adjusted to a pH of 6.7 and distributed anoxically in Hungate tubes.
258 Enrichment cultures were incubated at 36 °C. The growth was followed by optical density at
259 600 nm (Spectrophotometer, Spectronic Instruments, Spectronic 401).

260 Several strains were isolated from the last tube showing growth during the Most Probable
261 Number technique. The 15A and Recti_s6 strains were thus isolated from the medium
262 targeting the sulfate-reducers, whereas the 2A strain was isolated from the medium dedicated
263 to the fermentative metabolic group. Isolation of each strain was carried out by the method of
264 dilution series in deep agar (Pfennig and Trüper, 1992). Rifampicin was added at a
265 concentration of 10 µg/mL during the Recti_s6 isolation (Koelschbach et al., 2017). The
266 purity of the isolated strains was checked under a phase contrast microscope (BX60;
267 Olympus) as well as by sequencing their 16S rDNA genes. For the fermentative strains (2A &
268 Recti_S6), searching for the anaerobic fermentation products was conducted using 10 mM of
269 glucose and a N_2 gas phase (1 bar). The gas phase was followed by GC-µTCD (Micro GC
270 Fusion; Chemlys; France). The fermentation products were analyzed using ion
271 chromatography (ThermoFisher). This process was conducted at the end of the exponential
272 growth curve, by taking 0.5 mL of culture and filtering it at 0.22 µm (IC Millex®, Millipore)
273 in a sterile degassed Hungate tube. Sterile physiological water was added afterwards in order

to reach a final volume of 2 mL. For the sulfate-reducing strain (15A), the experiments were conducted in 120 mL penicillin flasks. The strain was cultivated with H_2/CO_2 (80/20, 1 bar) as energy and carbon sources respectively, in addition to 20 mM of sulfate as terminal electron acceptor. The final products obtained from the sulfate consumption by this strain were monitored in these conditions, then with 10 mM of formate as carbon and energy sources and 20 mM of sulfate under N_2 atmosphere. The changes in the gas and liquid phases were investigated by gas micro-chromatography and ion chromatography, respectively. The microbial growth was followed by optical density at 600 nm as described above. The isolated strains were tested for their oxygen tolerance. Different volumes of air, filtered at 0.1 µm, were added to several Bellco tubes. A tube with a nitrogen gas phase and another one containing only air served as controls. The gas phase was analyzed at the beginning and at the end of the experiment by a microthermal conductivity detector (Gc-µTCD; MicroGC Fusion; Chemlys; France). The microbial growth was followed by optical density at 600 nm.

2.8- Nucleic acids extraction and RNA retro-transcription.

At different times of the experiment, samples from the liquid phase were collected in order to co-extract the nucleic acids. The samples were directly filtered under vacuum using a 47 mm PES membrane filters of 0.1 µm porosity (by Sartorius Stedim). Afterwards, the collected filters were stored at -80 °C in order to protect the RNA. Filters were crushed in liquid nitrogen and the nucleic acids were extracted using the Fast RNA Prosoil Direct kit (MP BIO). DNA was separated from RNA with All Prep RNA/DNA (Qiagen) kit. From the isolated strains, 2 mL of each culture were pelleted by centrifugation at 10·000 g for 5 minutes. The DNA was then extracted using DNeasy Power Soil (Qiagen) kit. After extraction, DNA and RNA were quantified using the Quant-it^{TM} dsDNA HS (Invitrogen) and the Quant-it^{TM} RiboGreen (Invitrogen) kits, respectively. The measurements were done using a BioTEK SYNERGY HTX microplate reader. The reverse transcription of the RNA was

299 performed *via* retro transcriptase M-MLV (Invitrogen^{TM}) according to the supplier's
300 recommendations.

301 *2.9- Polymerase chain reaction and sequencing.*

302 The V3-V4 regions of the 16S rRNA gene of the genomic DNA and cDNA were amplified by
303 nested PCR as previously described (Yu et al., 2015). The search for archaeas was carried out
304 by targeting successively the 21F-958R and 349F-806R regions of the Archean 16S rRNA *via*
305 a nested PCR (Takai and Horikoshi, 2000). The Taq PCR Core Kit (Roche) and the 2720
306 Thermal Cycler (Applied Biosystems) were used. The bacterial PCR primer pairs (344F-
307 801R) that were used contained CTTTCCCTACACGACGCTCTTCCGATCT (forward) and
308 GGAGTTCAGACGTGTGCTCTTCCGATC (reverse) adapters. Afterwards, high-throughput
309 sequencing conducted by the GenoToul genomics platform (Toulouse, France), using
310 Illumina's MiSeq 2x250bp technology in accordance with the manufacturer's instructions was
311 undergone. Sequencing data were processed *via* FROGS analysis pipeline developed by the
312 GenoToul genomics plateform in the Galaxy interface (Escudié et al., 2018).

313 Using the DNA of the isolated strains, the 16S rRNA genes amplifications were conducted
314 with the primers set 8F-1489R (Lane, 1991; Weisburg et al., 1991). The amplicons were
315 sequenced by Qiagen Genomic Services (Sanger sequencing; Hilden, Germany).

316 Raw sequences were archived in public NCBI database (SAMN19579666-SAMN19579701).
317 The Genbank/ EMBL/ DDBJ accession numbers of the 16S rRNA gene sequences of isolated
318 strains were: 15A (MZ317661), Recti_s6 (MZ317662) and 2A (MZ317660).

319 *2.10- Quantitative PCR.*

320 Quantitative PCR (qPCR; Biorad CFX Connect) *via* Takyon NO ROX SYBR 2X MasterMix
321 blue dTTP (Eurogentec) was used to determine the number of 16S rRNA gene copies present
322 in each sample during the incubation at high pressure (from DNA and cDNA). The primers

used were 338F (Suzuki and Giovannoni, 1996) and 518R (Muyzer et al., 1993). All reactions had a 20µL final reaction volume in accordance with the supplier's instructions. The reactions were denatured at 95°C/3min followed by 40 cycles of 95°C/10sec, 55°C/20sec and 72°C/20sec. The number of copies was calculated starting from a standard with serially 10-fold diluted pCRTM 2.1-TOPO plasmid (TOPO TA cloning kit, Invitrogen).

2.11- X-Ray Tomography.

The morphological alterations of the solid phase were followed by X-ray tomography. Capillaries made of borosilicate with an internal diameter of 2 mm and a height of 3 cm were filled with the solid phase (sand) and positioned in the reactor. The bottom of each capillary was blocked with cotton to prevent loss of material. Before the experiment, capillaries were scanned by X-ray tomography for initial reference. After the completion of the experiment, the capillaries were removed and sealed at both ends with waterproof glue and stored at 4 °C in anaerobic glove-box until scanning. A Zeiss Xradia Versa 510 tomograph was used. Based on a prior sensitivity study, the selection of the acquisition parameters was centered on optimizing the image contrast, signal-to-noise ratio and acquisition duration. Typically a set of 1601 radiographies of 1024x1024 pixels with a pixel size of 2.5µm was acquired. The X-ray generator was operated at 40 kV and the exposure time of a single radiography is 10s. The set of recorded radiographs was reconstructed with XRM Reconstructor® (Zeiss, version 14) in order to obtain a stack of cross-sections forming a digital volume of the sample. This reconstruction software was based on the standard filtered back projection algorithm. The data were processed, visualized and interpreted using Dragonfly® (ORS, Version 2020.2.0.11731). A filtering step was first applied in order to improve the signal-to-noise ratio of the data. The subsequent segmentation step enabled the extraction of the different phases (solid, liquid, biomass) for further quantitative analyses such as assessment of the proportion and location of each phase in the studied volume and comparison of data sets before and after the experiment.

348 *2.12- X-Ray Diffraction and Scanning Electron Microscopy.*

349 X-Ray diffraction (XRD) was used to study the mineralogy of the reservoir rock. Mineral
350 identification was performed using a Bruker D2 Phaser powder diffractometer with a Cu Kα
351 radiation source. XRD patterns were recorded over 5° to 90° 2Θ with a 0.02° step and a 0.5 s
352 counting time per step. Samples from the reservoir rock were analyzed before the experiment.
353 Bulk rock was analyzed in order to obtain the global mineral phases and a color-based
354 fractionation was performed in order to identify potential minor crystallized phases. After the
355 completion of the reactor experiment, samples from different locations of the basket were
356 collected in the glove box. The collections were performed from three different depths that
357 were 1 cm away from each other. The samples were then dried up under gaseous N_2 in an
358 anaerobic glovebox at ambient temperature. All samples were manually ground and sieved
359 into a homogeneous powder at 100 µm, the product was then analyzed by XRD. Identification
360 of crystallized phases was done using the DIFFRAC.EVA software.

361 Scanning Electron Microscopy (SEM) was used to localize mineral phases and to detect
362 potential formation of biofilm. Collected samples from three different depths, that were 1 cm
363 away from each other, were immediately fixed in a mixture of cacodylate 0.1 M and 2.5 %
364 glutathione pH 7.2. They were then dried out in successive solutions containing 30 to 100 %
365 ethanol and finally evaporated using hexamethyldisilazane (HMDS). Afterwards, the samples
366 were mounted on stubs and platinum coated. Observations were carried out using a Gemini
367 SEM 300 (Zeiss) combined to Energy Dispersive Analysis (EDX) at 8 kV in secondary
368 electron mode (SE) or backscattering electron mode (BSE).

369

370 **3. Results**

371 *3.1- Monitoring of the physico-chemical evolution during abiotic experiments.*

After approximatively 10 days of mixing the liquid and the solid phases, water composition showed an increase of chloride (3.05 ± 0.15 mM), sulfate (0.29 ± 0.01 mM) and calcium (2.18 ± 0.22 mM) concentrations in the water, indicating that the mineral matrix released theses ions. Very limited quantity of acetate appeared in the liquid phase (0.005 ± 0.0003 mM). The solubilities at the thermodynamic equilibrium of the system liquid – solid – gas were calculated according to the measured variations in the liquid phase. Under a total pressure of 60 bar, a temperature of 36 °C and with a gas composition of 98.3% CH_4, 0.8% CO_2 and 0.9 % O_2 at equilibrium, the calculated solubility of CH_4, CO_2 and O_2 using PhreeqC and phreeqc.dat are $5.96 \cdot 10^{-2}$, $8.88 \cdot 10^{-3}$ and $5.25 \cdot 10^{-4}$ mol.Kgw^{-1}, respectively.

3.2- Monitoring of the physico-chemical evolution in the liquid phase during biotic experiment.

Throughout the experiment, liquid and gas samples were collected in order to perform the different analyses. The solid phase was analyzed before and after the experiment. The liquid phase was composed of the formation water with indigenous microorganisms. As expected from a deep aquifer formation water (- 582 m), the latter is highly reduced with an Eh around -200 mV (Table 1). The ionic water content is dominated by bicarbonate and sulfate amongst anions and calcium amongst cations. The total concentration of dissolved elements in the water can be estimated by summing bicarbonate, sulfate, chloride, calcium, magnesium, potassium and sodium knowing that 4.79 mM (286,6 mg.L^{-1}) represents only 0.8 % of seawater salinity (Banks et al., 2014). Such low salinity strongly suggests that the formation water is of meteoric origin. The concentrations of dissolved Ca^+ and HCO_3^- confirm an interaction between water and carbonate minerals such as lithoclasts observed in the reservoir rock. The origin of sulfate can be hardly depicted and could have resulted from the dissolution of trace amounts of gypsum or anhydrite or from oxidation of sulfides in more crucial conditions. Despite its relatively low concentration, the dominance of sulfate as a terminal

electron acceptor in the formation water suggests that sulfate-reducing bacteria are the dominant microorganisms in such ecosystem.

One month before its injection into the reactor, the formation water (downhole sample) containing the microorganisms, stored until now at 4°C, was supplemented with wellhead water, sterilized by 0.1µm-filtration and maintained at room temperature. At the beginning of the biotic experiment, sulfate concentration was $9.20 \cdot 10^{-2} \pm 4.60 \cdot 10^{-3}$ mM (*i.e.* $1.28 \cdot 10^{-1} \pm 6.40 \cdot 10^{-3}$ mmol; Figure 3a). During the experiment, analytical measurements showed an initial decrease in the amount of sulfate after 10 days from the start, followed by its complete consumption on day 32. In order to maintain the dynamic equilibrium, formation water supplemented with sulfate was added. The whole added formation water was filter-sterilized with a 0.1 µm filter to avoid any microbial interference. Three successive water injections were performed on days 48, 104 and 126, respectively. After each injection, an expected increase in sulfate quantity was noted. Sulfate quantity increased by $9.62 \cdot 10^{-2} \pm 4.81 \cdot 10^{-3}$ mmol, $5.10 \cdot 10^{-2} \pm 2.55 \cdot 10^{-3}$ mmol and $1.50 \cdot 10^{-2} \pm 7.50 \cdot 10^{-4}$ mmol on days 50, 105 and 131, respectively. Following these increases and before O_2 injection, sulfate consumption resumed and continued until sulfate's complete depletion from the system. During the first 130 days, $2.61 \cdot 10^{-1} \pm 1.31 \cdot 10^{-2}$ mmol of sulfate were consumed. The third injection was applied to refill the sulfate quantity in order to replenish the system stores before O_2 injection.

During this first period of the experiment, sulfate quantity showed a notable progressive reduction. However, after oxygen injection into the system, the previously noted progressive reduction in sulfate quantity was noted to subside and even reverse into a remarkable upsurge. This estimated increase in sulfate quantity was of $4.30 \cdot 10^{-2} \pm 2.15 \cdot 10^{-3}$ mmol. Using ionic chromatography coupled with a variable wavelength detector, no sulfide ions were detected in the liquid phase. Similarly no hydrogen sulfide was detected in the gas phase by gas chromatography (1 ppm as minimum detection limit). Taking into account the amount of

422 sulfate depleted from the system, sulfate-reducers were expected to produce $2.61 \cdot 10^{-1} \pm$
423 $1.31 \cdot 10^{-2}$ mmol of sulfide, bisulfide or hydrogen sulfide at most. Even if the sulfur was
424 supposedly only in the form of hydrogen sulfide, it constituted less than 0.006 % of the total
425 gas quantity. The value is too low to be detected by gas chromatography.

426 At the beginning of the experiment and simultaneously with sulfate consumption, an increase
427 in acetate quantity was noted and is shown in Figure 3b. Acetate was produced in the reactor
428 during the first 45 days despite not being detected initially in the formation water. Its quantity
429 increased from zero to $1.23 \pm 6 \cdot 10^{-2}$ mmol at day 13, then attained $2.09 \pm 1 \cdot 10^{-1}$ mmol at day
430 50 with an additional increase until reaching a peak of $2.34 \pm 1 \cdot 10^{-1}$ mmol. This quantity
431 remained stable until the end of the incubation.

432 Similarly to *in situ* conditions, mono-aromatic hydrocarbons including toluene and benzene
433 were supplemented in the gas phase. Monitoring of these compounds was carried out in the
434 liquid phase. At day 8, the molar quantity of toluene was around $2.55 \cdot 10^{-3} \pm 1 \cdot 10^{-4}$ mmol
435 (Figure3c), which decreased after 35 days before increasing again after toluene injection.
436 After this injection, $2.08 \cdot 10^{-3} \pm 1 \cdot 10^{-4}$ mmol were present in the system at day 49. Afterwards,
437 the toluene gradually decreased to $4.12 \cdot 10^{-4} \pm 6 \cdot 10^{-5}$ mmol at the end of the experiment (day
438 179). During 180 days of incubation including, 130 days in anaerobiosis and 50 days in
439 aerobiosis, no benzene degradation was observed in these conditions.

440

441 *3.3- Monitoring of the physico-chemical evolution in the gas phase during biotic experiment.*

442 Methane is the most abundant component in the gas phase. At the beginning of the
443 experiment, 60.4 ± 0.6 bar of the gas mixture CH_4 + 1% CO_2 was added to the system at a
444 temperature of 36 °C. Considering the compressibility factor of 0.9 which is calculated by the
445 PhreeqC model based on Peng-Robinson's equation, $4.52 \pm 2 \cdot 10^{-1}$ mol of CH_4 were injected.

446 At day 4, $5.99 \cdot 10^{-2} \pm 2x10^{-3}$ mol of CH_4 were lost from the gas phase (Figure 3d). Gas
447 quantities were calculated based on the total pressure measured by the barometer and the gas
448 phase composition analyzed by the gas chromatography. The calculation performed *via*
449 Phreeqc indicated a solubility of $6.25 \cdot 10^{-2}$ mol.Kgw^{-1} in this experiment's conditions. Thus,
450 taking into account the uncertainty, the CH_4 quantity lost from the gas phase corresponded
451 entirely to its soluble equivalent in the liquid phase. In order to readjust the total pressure after
452 stabilizing the piston position, a second and last injection of the gas mixture was performed
453 on day 6. This injection induced a $2.16 \cdot 10^{-1} \pm 1 \cdot 10^{-2}$ mol increase in methane quantity. After
454 each water injection, a certain number of methane moles transfer to the liquid phase in order
455 to preserve the gas-unsaturated liquid equilibrium. The quantities transferred to the formation
456 water were $6.27 \cdot 10^{-2} \pm 3 \cdot 10^{-3}$ mol, $7.77 \cdot 10^{-2} \pm 3 \cdot 10^{-3}$ mol and $7.13 \cdot 10^{-3} \pm 3 \cdot 10^{-4}$ mol after the
457 first, second and third water injections, respectively. Afterwards, no variations in methane
458 quantity were observed until the end of the experiment. The curve in the Figure 3d represents
459 the variations in methane quantity throughout the experiment based on the thermodynamic
460 model. This model fits well the experimental data obtained during the study.

461 Carbon dioxide was present in an initial proportion of 1 % of the gas mixture, corresponding
462 to an initial quantity of $4.56 \cdot 10^{-2} \pm 2 \cdot 10^{-3}$ mol in the gas phase. Figure 3e showed the
463 variations of CO_2 quantity during the experiment. Similarly, to methane, an initial decrease in
464 CO_2 quantity was observed due to the gas-liquid equilibrium. Following this phase, the
465 CH_4/CO_2 injection applied to readjust the pressure generated an increase in CO_2 quantity of
466 $2.34 \cdot 10^{-4} \pm 1 \cdot 10^{-5}$mol. Throughout the experiment, a decrease in CO_2 quantity was observed.
467 The last measurement that was done on day 178 showed $1.56 \cdot 10^{-2} \pm 7 \cdot 10^{-4}$ mol of CO_2 in the
468 gas phase. The curve representing the thermodynamic variations of CO_2 in the gas phase was
469 presented in the same figure. The model showed that the thermodynamic equilibrium and
470 gases solubility were reached before the reinjection of CH_4/CO_2. The reinjection did not have

any significant impact on the thermodynamic equilibrium in view of the minimal quantity that was added. The calculated pH was estimated at 5.1. However, the continuous decrease in the carbon dioxide quantity as well as the remarkable difference between the model and the experimental measurements cannot solely be explained by thermodynamic calculations and suggested the presence of an autotrophic metabolism and the incorporation of the carbon inside the biomass.

On day 130 of incubation, O_2 was injected in the reactor. At day 131, $4.16 \cdot 10^{-2} \pm 2 \cdot 10^{-3}$ mol were quantified, constituting 1% of the gas phase (Figure 3e). The quantity of oxygen is calculated based on the total pressure of the reactor with a compressibility factor of 0.9 and the molar fraction of O_2 analyzed by the gas chromatography. At the end of the experiment (day 178), $3.57 \cdot 10^{-2} \pm 1 \cdot 10^{-3}$ mol of O_2 remained in the gas mixture. Noting the increase in sulfate in the liquid phase after O_2 injection, 8.60 $x10^{-2}$ mmol of O_2 had potentially oxidized sulfide into sulfate. Calculated variations of O_2, taking into account the number of moles lost due to analysis, are represented in the curve. Note that the difference between the experimental and calculated values could be due to potential mineral oxidation that occurred in the reactor such as sulfur oxidation.

As previously explained, the experiment aims at studying the effects of the CH_4 -1% CO_2 -1% O_2 mixture in a deep storage aquifer. Hydrogen was not present in the injected gas mixture. However, limited quantities of H_2 near detection threshold were detected between day 4 and day 45 of the experiment as shown in Figure 3f. Before its depletion, the maximum measured quantity at day 31 was estimated at $2.51 \cdot 10^{-4} \pm 1 \cdot 10^{-5}$ mol, which represented 0.005% of the gas phase. In fact, this amount is too low to be considered at that time of the experiment. However, it is worth mentioning that the peak of H_2 was observed at a period when sulfate was undetected in the system. Surprisingly, H_2 accumulation clearly occurred after O_2 injection into the system. The amount of H_2 over time was shown through a

positive slope that started one day after oxygen injection and continued until the end of the experiment. The last measurement of H_2 in the gas phase was $1.99 \cdot 10^{-2} \pm 9 \cdot 10^{-4}$ mol, which represented 0.5% of the gas phase. The experimental H_2 values indicated continuous production of this gas. Considering a solubility of $2 \cdot 10^{-4}$ mol.Kgw^{-1} (*via* PhreeqC), $1.75 \cdot 10^{-4}$ mol of H_2 were present in the liquid phase at the end of the experiment.

3.4- Evolution of the bacterial community during the experiment.

Besides the importance of identifying O_2 effect on microbial life, analyzing the qualitative and quantitative variations in microbial diversity throughout the experiment can help understanding the changes in the liquid and the gas phases. The presence of archaea could not be demonstrated by PCR and nested-PCR approaches targeting this taxonomic group. The bacterial diversity results based on the sequencing of bacterial 16S rRNA genes were combined with the results of quantification of these same genes obtained by quantitative PCR in each sample (Figure 4). At the beginning of the experiment, the microbial community of $2.1 \cdot 10^5 \pm 1.3 \cdot 10^5$ cells/mL stored since five months at ambient pressure at 4 °C was dominated by *Geobacteraceae* > *Desulfovibrionaceae* > *Rhodocyclaceae* > *Spirochaetaceae*. The proportions of each of the aforementioned strain species were noted to vary during the first 43 days of incubation. On one hand a reduction in *Geobacteraceae* and *Desulfovibrionaceae* was observed, in contrast to a growth in *Spirochaetaceae* and *Peptococcaceae*. This new equilibrium in the community was relatively stable until incubation day 105 when the *Peptococcaceae* concentration was noted to be increasing. *Peptococcaceae* growth coincided with the reduction in toluene in the liquid phase (Figure 3c). The oxygen injection had a significant impact on the microbial community presented by a substantial reduction in the bacterial cell concentration from $1.1 \cdot 10^5 \pm 2.0 \cdot 10^4$ cells/mL (t_{130}) to $3.7 \cdot 10^3 \pm 1.2 \cdot 10^3$ cell/mL (t_{133}) reaching an endpoint of $4.1 \cdot 10^2 \pm 8.4 \cdot 10^1$ cell/mL (t_{179}). *Desulfovibrionaceae* and *Sphingomonodaceae* retained a detectable presence despite having

521 higher concentrations prior to oxygen injection. Members of the *Sphingomonodaceae* may
522 have aerobic metabolism in addition to having fermentation capacities allowing them to
523 produce H_2 by degrading organic molecules.

524 Via the 16S rRNA gene, the bacterial taxonomic diversity of active cells was monitored and
525 the results are presented in the Figure 5 and Table 2. The bacterial strains' activity seems to
526 be restricted and different from that seen at atmospheric pressure (intensity of activity at day 0
527 compared to the activity during the incubation). Thus, the *Geobacteraceae* (blue),
528 *Rhizobiaceae* (brown), *Desulfovibrionaceae* (black yellow, below) and *Spirochaetaceae* (dark
529 blue) were the most active in the original community obtained from the sampler that evolved
530 for several months at atmospheric pressure in anaerobiosis. Just before O_2 injection (day 130),
531 strong activities of *Desulfovibrionaceae* (yellow), *Peptococcaceae* (green) and
532 *Thermodesulfovibrionaceae* (blue) were detected. On day 179 at the end of the incubation and
533 even though their microbial activity were quite low, *Spirochaetaceae* and
534 *Desulfovibrionaceae* strains could still be detected. Hence, the sulfate-reducing metabolic
535 group had suffered but has not completely disappeared.

536 In addition, the liquid phase was sampled prior to O_2 injection in order to target and cultivate
537 sulfate-reducers and fermenters in special media, as those microorganisms are considered key
538 players in deep aquifers. From the sulfate-reducers' medium, the strain 15A, a representative
539 of the *Desulfovibrio vulgaris* strains, was isolated and identified (99.72% identity with 16S
540 rDNA sequence of *D. vulgaris* strain "Miyazaki F"). The strain 15A had a strictly anaerobic
541 growth. It was capable of growth with CO_2 and H_2 as sole carbon and energy sources.
542 Regarding its heterotrophic growth, formate oxidization was tested and turned to be
543 incomplete with noted production of acetate. As expected, the strain 15A did not produce
544 acetate when grown autotrophically. Two fermenters were isolated, strain 2A and strain
545 Recti_s6. Strain 2A is phylogenetically close to *Pleomorphomonas koreensis* (99.70% of

546 identity; 16S rDNA). Grown on glucose-based medium, strain 2A produces formate, acetate,
547 CO_2 and H_2 even in oxic conditions such as the air in the head space. Strain Recti_s6 is
548 related to *Rectinema cohabitans* strain HM (99.83% of identity) which a spirochaete isolated
549 from an anaerobic naphthalene-degrading enrichment culture (Koelschbach et al., 2017).
550 Finally, representatives of the *Bacillus* genus were also detected through the identification of
551 their characteristic structures and spore forms (data not shown). These bacteria are strictly
552 aerobic and are able to maintain under anoxic conditions through their ability to sporulate.
553 Spores protect these bacterial until more favorable conditions for germination occur.

554 *3.5- Evolution of the solid phase during the experiment.*

555 XRD was performed on the reservoir rock that is sampled from the deep aquifer and
556 introduced in the reactor and on the solid sample after the experiment. At the end of the
557 experiment, X-ray diffraction performed on the collected rock did not demonstrate any
558 significant changes in the solid crystallized phases before and after the experiment (Figure 6).
559 Mainly composed of quartz with minor calcite components, the solid sample did not vary
560 significantly after the experiment. However parallel measurements were performed on a
561 reservoir rock sample that was immerged in the formation water containing the microbial life
562 with the substitution of CH_4-CO_2-O_2 for N_2 gas. These measurements indicated the formation
563 of iron sulfide (Figure 6). Thus the possibility of iron sulfides production during the
564 experiment with its subsequent oxidation after O_2 injection cannot be excluded. SEM-EDX
565 showed high amount of clay minerals in between quartz grains, and Fe and S colocalization
566 suggested the presence of iron sulfides in agreement with XRD (Figure 7). No variations was
567 observed by depth in the basket and no biofilm could be detected in these conditions.

568 The average porosity obtained by means of X-ray tomography from four different capillaries
569 did not show any significant variation with an initial porosity of around 43.5 % and a final
570 one of around 44.5% with an estimated uncertainty of ± 2 %. Thus, no recrystallization or

potential biofilm could be demonstrated in agreement with mineralogical observations. Note that black particles were observed in the solid phase at the end of the experiment. Similar black particles produced during a bio-geochemical interactions study were identified as pyrite.

4. Discussion

The role and contribution of green and renewable energy in the energy mix is more than ever required in order to counteract and reduce the notorious effects of greenhouse gas emissions. As part of energy transition, natural gas will become greener through the production and storage of biomethane. However, despite that biomethane is an attractive source of renewable energy, the effects of its storage particularly in massive amounts remains unknown. Thus, identification and comprehension of associated phenomena to biomethane storage is fundamental for the basis of any territory's energy strategy. In order to secure energy supplies, to face consumption peaks and variations between summer and winter, a significant part of natural gas can be stored in geological structures such as salt cavities or deep aquifers. That said, biomethane could replace natural gas on the long term and can be stored within these geological structures. Unlike natural gas, O_2 is added to biomethane during sulfide reoxidation process before injection into the gas network. To our knowledge, this is the first study to evaluate the potential impact of O_2 in anoxic ecosystems such as deep aquifers in this setting. The scenario tested in this study is the most unfavorable case of biomethane storage consisting of an O_2 supply of 1% in the context of an Eocene aquifer which is mainly composed of sands, sandstones and carbonate deposits (Brenot et al., 2015). Based on the X-ray diffraction results, calcite, iron sulfides (pyrite and marcasite), oxi-hydroxides (maghemite and hematite) and clay minerals were detected in traces. The monitoring well Ab_L_1 sampled for this study is the closest to the natural gas bubble (Ranchou-Peyruse et al., 2019). At an approximate depth of 600 m, interactions between the formation water and the injected

596 gas are at their peak. Under a high pressure of 60 bar, oxygen solubility is more important
597 than its solubility at the surface even at a 1% proportion. The Ab_L_1 formation water has a
598 very low salinity of 4.79 mM (286.56 $mg.L^{-1}$) which is equivalent to only 0.8 % of marine
599 salinity (Table 1). However the abiotic experiment showed salt release from the solid into the
600 liquid phase despite rinsing of the rock during the preparation. Calcium and chloride were the
601 main ions detected. Calcium chloride is a brine known to be used during drilling operations.
602 Nevertheless, stoichiometry suggests another origin for calcium which could be released from
603 the calcite detected in the reservoir rock. Even in small quantities of few mmoles, changes in
604 the liquid's salinity have the potential to alter the thermodynamic equilibrium.

605 *4.1- Sampling and pre-incubation.*

606 The formation water containing indigenous microorganisms was sampled 5 months before the
607 start of the high-pressure biotic experiment. Water was collected using a downhole sampler
608 ensuring the purity of the microbiological sample and maintaining it under high-pressure until
609 reaching the laboratory. Under controlled conditions, the pressure was gradually lowered in
610 order to avoid damaging or destroying the microorganisms through rapid depressurization.
611 The formation water was then stored at ambient temperature and under anoxic conditions with
612 N_2 as gas phase. One month before the experiment, the formation water with the
613 microorganisms was supplemented with sterile water from the same study site in order to
614 reactivate the microorganisms. During this pre-incubation period, the microorganisms already
615 started to consume different elements present in the water particularly sulfate. Once injected
616 in the reactor, liquid phase was supplemented with sulfate by the release of these ions from
617 the rock. Sulfate ions present in the solid phase may be due to pyrite oxidation or to drilling
618 brines. Incubation at atmospheric pressure seems to have particularly favored the
619 *Geobacteraceae* family, which proportion drastically decreased in the pressurized reactor.
620 Similar changes affected the *Desulfovibrionaceae* family which are sulfate-reducing

proteobacteria previously described in this site (Ranchou-Peyruse et al., 2019). These findings encourage undergoing further studies assessing the behavior of microbial communities in deep environments under high pressures, even in continental undergrounds where pressures are known to be lower than deep marine ecosystems.

4.2- Physicochemical and bacterial evolution before oxygen injection.

The objective of the custom-designed reactor in this study is to simulate as precisely as possible a gas storage aquifer. Anoxic conditions were applied from the beginning of the experiment with a gas phase composed of CH_4 with 1% of CO_2 and small quantities of benzene and toluene. The entire rock was initially immersed in the formation water during the first 5 days in order to colonize it with microorganisms. Afterwards the water level was lowered allowing the upper part of the rock to bath in the gas phase whereas its lower part remained in the liquid phase with the microorganisms. Microbial communities were able to grow under a pressure of 60 bar and a temperature of 36 °C, similarly to the aquifer's *in situ* conditions. The thermodynamic modeling studies helped to identify the equilibrium status of our system. The parameters such as the gas quantity and volume, the aqueous phase composition and quantity and the temperature of the system were fixed. PhreeqC model calculated the solubility of each gas in the aqueous phase under the system's conditions, and the quantity of each gas in the gas phase at equilibrium. At day 5 and before the reinjection of CH_4+CO_2, the quantities of CH_4 ($4.46 \pm \cdot 2.2 \cdot 10^{-1}$ mol) and CO_2 ($2.97 \cdot 10^{-2} \pm 1.5 \cdot 10^{-3}$ mol) in the gas phase were equal to those calculated by PhreeqC (4.41 and $3.37 \cdot 10^{-2}$ mol), respectively. These findings confirm that the thermodynamic equilibrium was attained on day 5. The re-injection of the gas mixture on day 6 inducing a small increase in the quantities of these gases (Figures 2d and 2e) did not cause a significant difference in the thermodynamic equilibrium. On day 20, the reduction in CO_2 quantity from the gas phase was greater than the value calculated at the thermodynamic equilibrium suggesting an additional consumption

which can only be explained by integration of CO_2 in the bacterial biomass. The detection of H_2 followed by its consumption supports this hypothesis. Carbon dioxide and hydrogen are consumed by autotrophic microorganisms that use H_2 as a source of energy and electrons. The absence of archaea in the microbial community confirms the lack of CO_2/H_2 consumption *via* methanogenesis in this study. Since the beginning of the experiment, sulfate reduction was noted in the liquid phase in the absence of O_2. That observation necessitated three sulfate-supplemented formation water injections in order to maintain the incubation. The bacterial community analysis confirmed the presence of the *Desulfovibrionaceae* family (Figure 4). Moreover, the 16S rRNA transcripts studies confirmed their activity in the original community (Figure 5). Previous studies on the Ab_L_1 site recognized the activity of the sulfate-reducing bacteria, particularly the delta-proteobacteria which include the *Desulfovibrionaceae* family (Ranchou-Peyruse et al., 2019). We conclude that the anaerobic activity of sulfate-reducing bacteria was responsible for the depletion of sulfate from the system. The *Desulfovibrio vulgaris* 15A strain isolated in this study showed an ability to produce acetate under heterotrophic conditions. Acetate level was noted to increase during the first month of incubation and remained stable until the end of the experiment suggesting a simultaneous absence of acetoclastic bacteria (Figure 3b). Moreover, acetate was not among the ions released from the solid phase during the abiotic experiments. Acetate could have also been produced by fermentative bacteria present in the community such as isolated *Pleomophomonas koreensis* 2A and *Rectinema cohabitans* Recti_s6 strains. Under fermentative conditions, these two strains have been shown to produce formate, acetate, CO_2 and H_2. Therefore we conclude that in the first days of incubation, there was a significant activity of fermenters particularly *Spirochaetaceae* and heterotrophic sulfate-reducers. The latter reduce sulfate from organic molecules present in the water, mineral matrix but also in the necromass. It is also evident that the H_2 produced during fermentation was directly

consumed by the sulfate-reducers including the *Desulfovibrio vulgaris* 15A strain, as sulfate depletion coincided with H_2 detection. The hydrogenotrophic ability of certain strains of the *Desulfovibrio* genus has been previously reported (Bagnoud et al., 2016; Detmers et al., 2004). Conversely, sulfate supplementation resulted in H_2 disappearance. Similarly, the reduction in CO_2 (Figure 3e) could be partially explained by this autotrophic growth that uses this carbon source for its biomass and metabolism. However the sulfide compounds produced through the sulfate-reduction metabolism were not detected in the liquid nor the gas phases. The black particles observed in the solid basket and the reactor at the end of the experiment, identified as pyrite by XRD, suggest that iron sulfide was formed by the interaction of ferrous irons present in the reservoir rock and the formation water with the produced sulfide compounds (Berlendis et al., 2010; Caldwell et al., 2008; Fry et al., 1997; Park et al., 2006; Zettlitzer et al., 2010).

4.3- Monoaromatic hydrocarbons biodegradation.

Several studies have demonstrated the potential for biodegradation of monoaromatic hydrocarbons by autochthonous microbial communities in deep aquifers used for natural gas storage (Berlendis et al., 2010; Aüllo et al., 2016; Ranchou-Peyruse et al., 2017). In this study, the gas phase was supplemented with benzene and toluene at concentrations similar to those typically found in natural gas (7.95 ppm of benzene and 3.57 ppm of toluene). A reduction in toluene started around day 100 until the injection of O_2. No toluene reduction was noted in oxic conditions. A growth of the *Peptococcaceae* strains (Figures 4 and 5) can be noted in the same period. This bacterial family includes gram-positive sulfate-reducing and fermentative bacteria that have previously been associated with biodegradation of monoaromatic hydrocarbons in similar environments (Abu Laban et al., 2010; Aüllo et al., 2016; Kleinsteuber et al., 2008; Liu et al., 2004; Morasch et al., 2004; Ranchou-Peyruse et al., 2017; Robertson et al., 2000; Taubert et al., 2012). This hypothesis is consistent with the current

level of understanding of the behavior of microbial communities at the gas bubble / formation water interface. In close proximity to the gas bubble, exogenous molecules specifically carbon molecules transferred from the gas to the formation water become more accessible to the microorganisms. This zone that is less oligotrophic than the rest of the aquifer appears to be more favorable for the development of microorganisms such as *Desulfovibrio*. The *Desulfovibrio* genus is known to be more competitive and faster growing than *Desulfotomaculum* (*Peptococcaceae*) when present in environments with abundant organic molecules (Aüllo et al., 2013). After O_2 injection, a notable decline in sulfate reduction, microbial activity and toluene degradation were noted. Terminating the natural bio-attenuation of aromatic hydrocarbons could be a side effect of massive O_2 influx into UGS and should not be neglected in the management of these geological storages.

4.4- Evolution of the four-phase system after oxygen injection.

Once the O_2 was injected in the gas phase and based on abiotic physicochemical reactions, the simulation model predict that the value at saturation ($4.42 \cdot 10^{-4}$ mol.Kgw^{-1}) in the liquid phase was experimentally reached 5 days after the O_2 injection (*i.e.*, t_{136}). However, the experimental data showed a constant decrease in the gas phase of O_2 until the end of the experiment. This reduction is linked to: i) the solubilization of O_2 in the liquid phase (0.67 mmol estimated from the model); ii) the reoxidation of sulfide into sulfate (8.60×10^{-2} mmol), the sulfide potentially trapped in the form of iron sulfides in the rock matrix (*e.g.* pyrite). Many studies showed the immediate underground oxidation of pyrite after O_2 injection in the storage systems (Guo et al., 2021; Kushnir et al., 2012; Lu et al., 2016; Vu et al., 2018) causing an increase in sulfate quantities (Yuan et al., 2009); iii) and a possible reoxidation of other reduced elements, such as ferrous ions. The decrease in O_2 quantity was more significant and may be due to different gas-solid interactions not identified during our study. The solubility of O_2 simulated by the model can be estimated to be around $4.42 \cdot 10^{-4}$

721 mol.Kgw^{-1} in the liquid phase during the last 50 days of the experiment. If a comparable water
722 is placed under different environment and conditions such as air and 36 °C temperature, O_2
723 saturation would be of around $2.1 \cdot 10^{-4}$ mol.Kgw^{-1} at equilibrium (Benson and Krause, 1980;
724 Millero et al., 2002) and an aerobic microbial ecosystem would develop (Stiff et al., 1992).
725 The hyperoxic water in our reactor was clearly toxic to the strictly anaerobic microorganisms,
726 as evidenced by the drastic decrease in bacterial taxonomic diversity and its activity from the
727 day following O_2 injection (Figures 4 and 5) even if the existence of some anoxic micro-
728 niches could be supposed. It is probable that part of O_2 could have reacted with the organic
729 matter resulting from necromass.

730 Some microorganisms survived these new environmental conditions and retained a metabolic
731 activity as demonstrated by a surprising constant production of H_2 following O_2 injection that
732 persists till the end of the experiment. Analyses performed on fermentative strains 2A and
733 Recti_s6 demonstrated their capability to produce H_2 in oxic conditions. With the reduction in
734 the majority of strict anaerobic bacteria and the decline in hydrogenotrophic sulfate-reducers
735 such as *Desulfovibrio vulgaris* 15A, sulfate and H_2 were no longer consumed, explaining its
736 accumulation in the gas phase. Despite that some strains of the *Desulfovibrionaceae* family
737 were able to survive O_2, their activity is significantly slow and even negligible. A study
738 conducted by Yuan et al. showed the occurrence of sulfate-reduction in anaerobic
739 environment after undergoing phases of oxygen stress. Sulfate-reducing bacteria can have a
740 relative temporary resistance to oxic environments (Yuan et al., 2009) which explains the
741 detection of their low activity. It is possible that some aerobic microorganisms such as
742 *Bacillus* strains and/or aero-anaerobic microorganisms such as *Sphingomonadaceae* may have
743 consumed some of the O_2 as well (Kosako et al., 2000).

744 Despite that the solid phase demonstrated no changes in porosity % or mineral composition
745 among others, the pre and post experimental analyses cannot completely rule out the

746 possibility of potential changes secondary to O_2 injection in the UGS. In fact, the reservoir
747 rock sample was in contact with O_2 present in the air before the experiment and was scanned
748 by X-ray tomography and XRD in oxic conditions. During the experiment, interactions
749 occurred in anoxic environment and produce minerals such as metal sulfides. Following O_2
750 injection, changes such as mineral oxidation occurred. At this stage, the solid phase was in
751 oxic conditions, similarly to its state before the beginning of the experiment. There were no
752 signs suggesting that the metal sulfides precipitates could have significantly reduced the
753 porosity of the rock prior to oxygen injection. However considering these facts, further studies
754 are required in order to assess the state of the solid phase after incubation and before O_2
755 injection in the system.

756 During the multidisciplinary experiment, oxygen effects on the different phases of an aquifer
757 during biomethane storage were assessed. Oxygen injection induced mineral oxidation to the
758 reservoir rock (Lu et al., 2016; Vu et al., 2018), especially iron sulfide oxidation causing
759 increase in sulfate concentration in the aqueous phase. In fact, iron sulfide oxidation was
760 already observed during CAES (Guo et al., 2021; Jung et al., 2013) and CCS (Jung et al.,
761 2013; Shao et al., 2014; Wei et al., 2015) where oxygen was injected as impurity. On a larger
762 scale, reaction of minerals and their dissolution in the aqueous phase can alter the reservoir
763 rock's porosity and therefore affect the storage volume. Another clear result obtained was the
764 deleterious effect of oxygen on the anaerobic microbial communities. Many studies were
765 conducted to confirm the capability of these communities to underground biodegrade
766 hydrocarbons, especially the sulfate-reducing bacteria (Aüllo et al., 2013; Ranchou-Peyruse et
767 al., 2019). Even though the microbial concentration drastically decreased after O_2 injection,
768 some of the communities were able to survive. In order to develop, those communities might
769 adapt to the new aquifer conditions. To get their needs of carbon, microorganisms might
770 develop capabilities for hydrocarbon biodegradation and therefore, the microbial community

771 would adapt to their new environment. During CCS or biomethane storage in deep aquifers,
772 oxygen's effects should be considered on many levels depending on the storage conditions
773 such as the reservoir rock's composition and the microbial communities harbored *in-situ*.

774 **5. Conclusion**

775 In this experiment, we were able to simulate the aquifer Ab_L_1 situated in South Aquitaine,
776 Southwest France in a reactor. Through a multidisciplinary approach, the impact of 1% of O_2
777 under 60 bar total pressure was evaluated in a UGS aquifer for the first time ever. The
778 relatively simple composition of the rock matrix at the Ab_L_1 site mainly containing sand
779 and to a lesser degree calcite did not seem to react after the addition of O_2 at low
780 concentration. Reoxidation of metal sulfide precipitates was expected with subsequent
781 minimal increase in the porosity of the aquifer rock. As of the early 1990s, sulfate was noted
782 to decrease in the Ab_L_1 site as a result of the sulfate-reducing activity amplified by the
783 proximity of the gas bubble and by the consumption of organic molecules dissolved in water
784 by sulfate-reducers (1992: ≈18 mg/L SO_4^{2-}, 2013: <7 mg/L SO_4^{2-};(Ranchou-Peyruse et al.,
785 2019)). The reoxidation of metal sulfides would therefore contribute to the restoration of
786 higher sulfate concentrations. Similarly the direct effect on the gases stored in the aquifer
787 (99% CH_4, 1% CO_2) seemed negligible and even absent. Conversely, O_2 had a deleterious
788 effect on the strictly anaerobic microbial community interacting with the UGS. This effect
789 manifested as a decline and even a complete arrest of the natural bioattenuation of
790 monoaromatic hydrocarbons, a decrease in oxygen amount and finally a surprising H_2
791 accumulation in the gas phase deriving from fermentative bacteria able to survive the new
792 oxic conditions.

793 The different biological, geological and chemical impacts of biomethane storage containing
794 1% of O_2 as impurity were evaluated in this study. It will be necessary to carry out new
795 studies with lower oxygen concentrations and for other storage conditions (temperature,

pressure, rocks). Nevertheless, in view of these first results, the elimination of oxygen from the gas mixture before its injection must be considered. However oxygen is widely used during different stages of the processing of various other resources such as in CCS or CAES in geological sites. The findings noted in our study shed a new light on O_2 gas effects on the underground environment which is an important step in the green energy era. Such observations lay the cornerstone for the future selection of accessible, secure and stable ways of biomethane underground storage which is crucial for building a successful global clean energy strategy. Further studies involving the use of various amounts of oxygen during storage of different gases compositions and their subsequent implications are required for a better understanding of the static and dynamic interactions occurring during gas storage practices.

Acknowledgments

Enagas, SNAM, Storengy and Teréga are acknowledged for funding this research project. We are grateful to the Genotoul platform (genotoul.fr) for the sequencing analyses. MRP salary was supported by E2S-UPPA. We would also like to thank Total for providing UMS 3360 DMEX with the Zeiss Xradia Versa 510 which carried out the tomographic acquisitions reported in this article.

Author Contributions Statement

FC, MRP, PC and ARP co-conceived the study. PH, JM, FC, PC carried out the high pressure and simulation experiments. MG, MRP and ARP applied the microbiological approaches. PS, M-PI, IS, PM and GH used the imaging and mineralogical characterization. ML and ILH analyzed the hydrocarbons. All authors contributed in the interpretation of results and paper writing.

Declaration of interests

DD and PCh are employed by two French companies specialized in geological natural gas storage which are Storengy and Teréga respectively.

Conflict of interest

No conflict of interest declared in relation to the work described.

825 **References**

826 Abu Laban, N., Selesi, D., Rattei, T., Tischler, P., Meckenstock, R.U., 2010. Identification of
827 enzymes involved in anaerobic benzene degradation by a strictly anaerobic iron-
828 reducing enrichment culture: Enzymes involved in anaerobic benzene degradation.
829 Environmental Microbiology no-no. https://doi.org/10.1111/j.1462-
830 2920.2010.02248.x
831 Aüllo, T., Berlendis, S., Lascourrèges, J.-F., Dessort, D., Duclerc, D., Saint-Laurent, S.,
832 Schraauwers, B., Mas, J., Patriarche, D., Boesinger, C., Magot, M., Ranchou-Peyruse,
833 A., 2016. New Bio-Indicators for Long Term Natural Attenuation of Monoaromatic
834 Compounds in Deep Terrestrial Aquifers. Frontiers in Microbiology 7.
835 https://doi.org/10.3389/fmicb.2016.00122
836 Aüllo, T., Ranchou-Peyruse, A., Ollivier, B., Magot, M., 2013. Desulfotomaculum spp. and
837 related gram-positive sulfate-reducing bacteria in deep subsurface environments.
838 Frontiers in Microbiology 4. https://doi.org/10.3389/fmicb.2013.00362
839 Banks, D., Kadnikov, V.V., Franck, 2014. Hydrochemical data report from sampling of two
840 deep abandoned hydrocarbon exploration wells: Byelii Yar and Parabel', Tomsk
841 oblast', western Siberia, Russian Federation. (No. 2014.034). Geological Survey of
842 Norway.
843 Barik, D., Sah, S., Murugan, S., 2013. BIOGAS PRODUCTION AND STORAGE FOR
844 FUELING INTERNAL COMBUSTION ENGINES 3, 10.
845 Benson, B.B., Krause, D., 1980. The concentration and isotopic fractionation of gases
846 dissolved in freshwater in equilibrium with the atmosphere. 1. Oxygen: Oxygen in
847 freshwater. Limnology and Oceanography 25, 662–671.
848 https://doi.org/10.4319/lo.1980.25.4.0662
849 Berlendis, S., Lascourreges, J.-F., Schraauwers, B., Sivadon, P., Magot, M., 2010. Anaerobic
850 Biodegradation of BTEX by Original Bacterial Communities from an Underground
851 Gas Storage Aquifer. Environmental Science & Technology 44, 3621–3628.
852 https://doi.org/10.1021/es100123b
853 Bombach, P., Chatzinotas, A., Neu, T.R., KÃ¤stner, M., Lueders, T., Vogt, C., 2010.
854 Enrichment and characterization of a sulfate-reducing toluene-degrading microbial
855 consortium by combining *in situ* microcosms and stable isotope probing techniques.
856 FEMS Microbiology Ecology 71, 237–246. https://doi.org/10.1111/j.1574-
857 6941.2009.00809.x
858 Brenot, A., Négrel, P., Petelet-Giraud, E., Millot, R., Malcuit, E., 2015. Insights from the
859 salinity origins and interconnections of aquifers in a regional scale sedimentary aquifer
860 system (Adour-Garonne district, SW France): Contributions of δ34S and δ18O from
861 dissolved sulfates and the 87Sr/86Sr ratio. Applied Geochemistry 53, 27–41.
862 https://doi.org/10.1016/j.apgeochem.2014.12.002
863 Cai, M., Yu, C., Wang, R., Si, Y., Masakorala, K., Yuan, H., Yao, J., Zhang, J., 2015. Effects
864 of oxygen injection on oil biodegradation and biodiversity of reservoir
865 microorganisms in Dagang oil field, China. International Biodeterioration &
866 Biodegradation 98, 59–65. https://doi.org/10.1016/j.ibiod.2014.12.003
867 Caldwell, S.L., Laidler, J.R., Brewer, E.A., Eberly, J.O., Sandborgh, S.C., Colwell, F.S.,
868 2008. Anaerobic Oxidation of Methane: Mechanisms, Bioenergetics, and the Ecology
869 of Associated Microorganisms. Environmental Science & Technology 42, 6791–6799.
870 https://doi.org/10.1021/es800120b
871 Detmers, J., Strauss, H., Schulte, U., Bergmann, A., Knittel, K., Kuever, J., 2004. FISH
872 Shows That Desulfotomaculum spp. Are the Dominating Sulfate-Reducing Bacteria in
873 a Pristine Aquifer. Microbial Ecology 47. https://doi.org/10.1007/s00248-004-9952-6

Eichler, B., Pfennig, N., 1986. Characterization of a new platelet-forming purple sulfur bacterium, Amoebobacter pedioformis sp. nov. Archives of Microbiology 146, 295–300. https://doi.org/10.1007/BF00403233

EPA, 2017. How to evaluate alternativecleanup technologies for underground storage tank sites (No. EPA 510-B-17-003). EPA (United States Environmental Protection Agency).

Escudié, F., Auer, L., Bernard, M., Mariadassou, M., Cauquil, L., Vidal, K., Maman, S., Hernandez-Raquet, G., Combes, S., Pascal, G., 2018. FROGS: Find, Rapidly, OTUs with Galaxy Solution. Bioinformatics 34, 1287–1294. https://doi.org/10.1093/bioinformatics/btx791

Fry, N.K., Fredrickson, J.K., Fishbain, S., Wagner, M., Stahl, D.A., 1997. Population structure of microbial communities associated with two deep, anaerobic, alkaline aquifers. Applied and environmental microbiology 63, 1498–1504. https://doi.org/10.1128/AEM.63.4.1498-1504.1997

Guo, C., Li, C., Zhang, K., Cai, Z., Ma, T., Maggi, F., Gan, Y., El-Zein, A., Pan, Z., Shen, L., 2021. The promise and challenges of utility-scale compressed air energy storage in aquifers. Applied Energy 286, 116513. https://doi.org/10.1016/j.apenergy.2021.116513

Itävaara, M., Nyyssönen, M., Kapanen, A., Nousiainen, A., Ahonen, L., Kukkonen, I., 2011. Characterization of bacterial diversity to a depth of 1500 m in the Outokumpu deep borehole, Fennoscandian Shield: Deep terrestrial biodiversity. FEMS Microbiology Ecology 77, 295–309. https://doi.org/10.1111/j.1574-6941.2011.01111.x

Jung, H.B., Um, W., Cantrell, K.J., 2013. Effect of oxygen co-injected with carbon dioxide on Gothic shale caprock–CO2–brine interaction during geologic carbon sequestration. Chemical Geology 354, 1–14. https://doi.org/10.1016/j.chemgeo.2013.06.019

Kampman, N., Bickle, M.J., Maskell, A., Chapman, H.J., Evans, J.P., Purser, G., Zhou, Z., Schaller, M.F., Gattacceca, J.C., Bertier, P., Chen, F., Turchyn, A.V., Assayag, N., Rochelle, C., Ballentine, C.J., Busch, A., 2014. Drilling and sampling a natural CO2 reservoir: Implications for fluid flow and CO2-fluid–rock reactions during CO2 migration through the overburden. Chemical Geology 369, 51–82. https://doi.org/10.1016/j.chemgeo.2013.11.015

Kleinsteuber, S., Schleinitz, K.M., Breitfeld, J., Harms, H., Richnow, H.H., Vogt, C., 2008. Molecular characterization of bacterial communities mineralizing benzene under sulfate-reducing conditions: Benzene mineralization under sulfate-reducing conditions. FEMS Microbiology Ecology 66, 143–157. https://doi.org/10.1111/j.1574-6941.2008.00536.x

Koelschbach, J.S., Mouttaki, H., Pickl, C., Heipieper, H.J., Rachel, R., Lawson, P.A., Meckenstock, R.U., 2017. Rectinema cohabitans gen. nov., sp. nov., a rod-shaped spirochaete isolated from an anaerobic naphthalene-degrading enrichment culture. International Journal of Systematic and Evolutionary Microbiology 67, 1288–1295. https://doi.org/10.1099/ijsem.0.001799

Koenen, M., Tambach, T.J., Neele, F.P., 2011. Geochemical effects of impurities in CO2 on a sandstone reservoir. Energy Procedia 4, 5343–5349. https://doi.org/10.1016/j.egypro.2011.02.516

Kosako, Y., Yabuuchi, E., Naka, T., Fujiwara, N., Kobayashi, K., 2000. Proposal of Sphingomonadaceae fam. nov., consisting of Sphingomonas Yabuuchi et al. 1990, Erythrobacter Shiba and Shimidu 1982, Erythromicrobium Yurkov et al. 1994, Porphyrobacter Fuerst et al. 1993, Zymomonas Kluyver and van Niel 1936, and Sandaracinobacter Yurkov et al. 1997, with the type genus Sphingomonas Yabuuchi et al. 1990. Microbiology and immunology 44, 563–575.

Kushnir, R., Ullmann, A., Dayan, A., 2012. Thermodynamic and hydrodynamic response of compressed air energy storage reservoirs: a review. Reviews in Chemical Engineering 28. https://doi.org/10.1515/revce-2012-0006

Lane, D.J., 1991. 16S/23S rRNA sequencing. Nucleic acid techniques in bacterial systematics 115–175.

Lei, H., Li, J., Li, X., Jiang, Z., 2016. Numerical modeling of co-injection of N 2 and O 2 with CO 2 into aquifers at the Tongliao CCS site. International Journal of Greenhouse Gas Control 54, 228–241. https://doi.org/10.1016/j.ijggc.2016.09.010

Lien, P.J., Yang, Z.H., Chang, Y.M., Tu, Y.T., Kao, C.M., 2016. Enhanced bioremediation of TCE-contaminated groundwater with coexistence of fuel oil: Effectiveness and mechanism study. Chemical Engineering Journal 289, 525–536. https://doi.org/10.1016/j.cej.2016.01.011

Liu, A., Garcia-Dominguez, E., Rhine, E.., Young, L.., 2004. A novel arsenate respiring isolate that can utilize aromatic substrates. FEMS Microbiology Ecology 48, 323–332. https://doi.org/10.1016/j.femsec.2004.02.008

Liu, Y.-F., Galzerani, D.D., Mbadinga, S.M., Zaramela, L.S., Gu, J.-D., Mu, B.-Z., Zengler, K., 2018. Metabolic capability and in situ activity of microorganisms in an oil reservoir. Microbiome 6. https://doi.org/10.1186/s40168-017-0392-1

Lu, J., Mickler, P.J., Nicot, J.-P., Yang, C., Darvari, R., 2016. Geochemical impact of O 2 impurity in CO 2 stream on carbonate carbon-storage reservoirs. International Journal of Greenhouse Gas Control 47, 159–175. https://doi.org/10.1016/j.ijggc.2016.01.039

Millero, F.J., Huang, F., Laferiere, A.L., 2002. Solubility of oxygen in the major sea salts as a function of concentration and temperature. Marine Chemistry 78, 217–230. https://doi.org/10.1016/S0304-4203(02)00034-8

Morasch, B., Schink, B., Tebbe, C.C., Meckenstock, R.U., 2004. Degradation of o -xylene and m -xylene by a novel sulfate-reducer belonging to the genus Desulfotomaculum. Archives of Microbiology 181, 407–417. https://doi.org/10.1007/s00203-004-0672-6

Morgan, H., Large, D., Bateman, K., Hanstock, D., Gregory, S., 2017. The Effect of Variable Oxygen Impurities on Microbial Activity in Conditions Resembling Geological Storage Sites. Energy Procedia 114, 3077–3087. https://doi.org/10.1016/j.egypro.2017.03.1437

Muyzer, G., de Waal, E.C., Uitterlinden, A.G., 1993. Profiling of complex microbial populations by denaturing gradient gel electrophoresis analysis of polymerase chain reaction-amplified genes coding for 16S rRNA. Applied and Environmental Microbiology 59, 695–700. https://doi.org/10.1128/AEM.59.3.695-700.1993

Pannekens, M., Kroll, L., Müller, H., Mbow, F.T., Meckenstock, R.U., 2019. Oil reservoirs, an exceptional habitat for microorganisms. New Biotechnology 49, 1–9. https://doi.org/10.1016/j.nbt.2018.11.006

Park, J., Sanford, R.A., Bethke, C.M., 2006. Geochemical and microbiological zonation of the Middendorf aquifer, South Carolina. Chemical Geology 230, 88–104. https://doi.org/10.1016/j.chemgeo.2005.12.001

Parkhurst, D.L., Appelo, C.A.J., 1999. User's guide to PHREEQC (Version 2): a computer program for speciation reaction-path, 1D-transport, and inverse geochemical calculations (No. 312). U.S. Geological Survey Water-Resources Investigations.

Pfennig, N., Trüper, H.G., 1992. The family Chromatiacea, in: The Prokaryotes. Springer, New York, NY.

Pfennig, N., Widdel, F., Trüper, H.G., 1981. The Dissimilatory Sulfate-Reducing Bacteria, in: Starr, M.P., Stolp, H., Trüper, H.G., Balows, A., Schlegel, H.G. (Eds.), The Prokaryotes. Springer Berlin Heidelberg, Berlin, Heidelberg, pp. 926–940. https://doi.org/10.1007/978-3-662-13187-9_74

Ranchou-Peyruse, M., Auguet, J.-C., Mazière, C., Restrepo-Ortiz, C.X., Guignard, M., Dequidt, D., Chiquet, P., Cezac, P., Ranchou-Peyruse, A., 2019. Geological gas-storage shapes deep life. Environmental Microbiology. https://doi.org/10.1111/1462-2920.14745

Ranchou-Peyruse, M., Gasc, C., Guignard, M., Aüllo, T., Dequidt, D., Peyret, P., Ranchou-Peyruse, A., 2017. The sequence capture by hybridization: a new approach for revealing the potential of mono-aromatic hydrocarbons bioattenuation in a deep oligotrophic aquifer. Microbial Biotechnology 10, 469–479. https://doi.org/10.1111/1751-7915.12426

Renard, S., Sterpenich, J., Pironon, J., Chiquet, P., Randi, A., 2014. Geochemical effects of an oxycombustion stream containing SO2 and O2 on carbonate rocks in the context of CO2 storage. Chemical Geology 382, 140–152. https://doi.org/10.1016/j.chemgeo.2014.05.032

Robertson, W.J., Franzmann, P.D., Mee, B.J., 2000. Spore-forming, Desulfosporosinus-like sulphate-reducing bacteria from a shallow aquifer contaminated with gasolene. Journal of Applied Microbiology 88, 248–259. https://doi.org/10.1046/j.1365-2672.2000.00957.x

Scarlat, N., Dallemand, J.-F., Fahl, F., 2018. Biogas: Developments and perspectives in Europe. Renewable Energy 129, 457–472. https://doi.org/10.1016/j.renene.2018.03.006

Shao, H., Kukkadapu, R.K., Krogstad, E.J., Newburn, M.K., Cantrell, K.J., 2014. Mobilization of metals from Eau Claire siltstone and the impact of oxygen under geological carbon dioxide sequestration conditions. Geochimica et Cosmochimica Acta 141, 62–82. https://doi.org/10.1016/j.gca.2014.06.011

Stiff, M.J., Cartwright, N.G., Crane, R.I., 1992. ENVIRONMENTAL QUALITY STANDARDS FOR DISSOLVED OXYGEN 132.

Suzuki, M.T., Giovannoni, S.J., 1996. Bias caused by template annealing in the amplification of mixtures of 16S rRNA genes by PCR. Applied and environmental microbiology 62, 625–630. https://doi.org/10.1128/AEM.62.2.625-630.1996

Takai, K., Horikoshi, K., 2000. Rapid Detection and Quantification of Members of the Archaeal Community by Quantitative PCR Using Fluorogenic Probes. Applied and Environmental Microbiology 66, 5066–5072. https://doi.org/10.1128/AEM.66.11.5066-5072.2000

Taubert, M., Vogt, C., Wubet, T., Kleinsteuber, S., Tarkka, M.T., Harms, H., Buscot, F., Richnow, H.-H., von Bergen, M., Seifert, J., 2012. Protein-SIP enables time-resolved analysis of the carbon flux in a sulfate-reducing, benzene-degrading microbial consortium. The ISME Journal 6, 2291–2301. https://doi.org/10.1038/ismej.2012.68

Trulli, E., Morosini, C., Rada, E., Torretta, V., 2016. Remediation in Situ of Hydrocarbons by Combined Treatment in a Contaminated Alluvial Soil due to an Accidental Spill of LNAPL. Sustainability 8, 1086. https://doi.org/10.3390/su8111086

Vu, H.P., Black, J.R., Haese, R.R., 2018. The geochemical effects of O2 and SO2 as CO2 impurities on fluid-rock reactions in a CO2 storage reservoir. International Journal of Greenhouse Gas Control 68, 86–98. https://doi.org/10.1016/j.ijggc.2017.11.001

Wang, J., Ryan, D., Anthony, E.J., Wildgust, N., Aiken, T. 2011. Effects of impurities on CO2 transport, injection and storage. Energy Procedia 4 2214-2221.Wei, N., Li, X., Wang, Y., Zhu, Q., Liu, S., Liu, N., Su, X., 2015. Geochemical impact of aquifer storage for impure CO 2 containing O 2 and N 2 : Tongliao field experiment. Applied Energy 145, 198–210. https://doi.org/10.1016/j.apenergy.2015.01.017

Weisburg, W.G., Barns, S.M., Pelletier, D.A., Lane, D.J., 1991. 16S ribosomal DNA amplification for phylogenetic study. Journal of Bacteriology 173, 697–703. https://doi.org/10.1128/JB.173.2.697-703.1991

Widdel, F., Bak, F., 1992. Gram-Negative Mesophilic Sulfate-Reducing Bacteria, in: Balows, A., Trüper, H.G., Dworkin, M., Harder, W., Schleifer, K.-H. (Eds.), The Prokaryotes. Springer New York, New York, NY, pp. 3352–3378. https://doi.org/10.1007/978-1-4757-2191-1_21

Yu, G., Fadrosh, D., Goedert, J.J., Ravel, J., Goldstein, A.M., 2015. Nested PCR Biases in Interpreting Microbial Community Structure in 16S rRNA Gene Sequence Datasets. PLOS ONE 10, e0132253. https://doi.org/10.1371/journal.pone.0132253

Yuan, Y., Conrad, R., Lu, Y., 2009. Responses of methanogenic archaeal community to oxygen exposure in rice field soil: Response of methanogens to aeration in rice soil. Environmental Microbiology Reports 1, 347–354. https://doi.org/10.1111/j.1758-2229.2009.00036.x

Zettlitzer, M., Moeller, F., Morozova, D., Lokay, P., Würdemann, H., 2010. Re-establishment of the proper injectivity of the CO2-injection well Ktzi 201 in Ketzin, Germany. International Journal of Greenhouse Gas Control 4, 952–959. https://doi.org/10.1016/j.ijggc.2010.05.006

1042 **Tables and Figures**

1043 **Table 1** - Physico-chemical parameters and compounds of the formation water sampled from
1044 the deep aquifer (Ab_L_1 site), analyzed at atmospheric pressure.

1045 **Table 2-** Standard deviation related to the 16S rRNA transcripts

1046 **Figure 1** - Scheme of the experimental apparatus used during the experiment.

1047 **Figure 2-** Diagram representing the different steps and analyses undergone though the biotic
1048 experiment.

1049 **Figure 3**- Results of the liquid and gas analyses during the biotic high pressure experiment
1050 (60 bar). The vertical line at day 6 represents the CH_4+CO_2 reinjection. The vertical dotted
1051 lines at days 48, 104 and 126 represent sulfate injections. The vertical line at day 132
1052 represents the oxygen injection. a) Sulfate variation in the liquid phase; b) Acetate variation in
1053 the liquid phase; c) Toluene (represented by the blue squares) and benzene (represented by the
1054 red triangles) variations in the liquid phase. The vertical line at day 47 represents toluene
1055 injection. d) Methane variation in the gas phase. The red dots and line represent the calculated
1056 values; e) Carbon dioxide (represented by the green squares) and oxygen (represented by the
1057 red triangles) variations in the gas phase). The lines represent the calculated values; f)
1058 Hydrogen variation in the gas phase.

1059 **Figure 4**- Evolution of the bacterial community during the incubation at 60 bar, 36°C and
1060 with a gas mixture (CH_4, 1%CO_2, 7.95ppm of benzene and 3.57 ppm of toluene) before and
1061 after oxygen injection (1%). The taxonomic diversity is monitored by 16S rRNA genes
1062 sequencing and the quantification is estimated by qPCR of 16S rDNA gene copies for each ml
1063 of sampled water through the experiment. 3a) Monitoring over the 180 days of the
1064 experiment. Following the oxygen injection, the quantity of microorganisms has drastically
1065 decreased. In order to observe the taxonomic diversity, the boxed part is zoomed in figure 3b.

1066 The variation of the sulfate quantity in the liquid phase is represented by the orange dots.
1067 Figure 3b- represents a zoom in on results after O_2 injection.

1068 **Figure 5**- Evolution of the active bacterial community (during the incubation at 60 bar, 36°C
1069 with a gas mixture (CH_4, 1%CO2, 7.95 ppm of benzene and 3.57 ppm of toluene) before and
1070 after oxygen injection (1%). The taxonomic diversity is based on the sequencing of cDNA of
1071 the 16S RDNA copies and the quantification was estimated by qPCR of cDNA for each mL
1072 of sampled water through the experiment.

1073 **Figure 6-** X-ray diffraction patterns of samples collected before the experiment (T0) and after
1074 the experiment at three depths (top, middle, bottom). I: illite, K: kaolinite, M: maghemite, Q:
1075 quartz, C: calcite, Ms: marcassite, P: pyrite.

1076 **Figure 7-** SEM-EDX observations from surface samples collected at the end of experiment
1077 showing clay minerals and quartz (A, SE mode)) and observation of iron sulfides (B, BSE
1078 mode).

1079

The different components:

1- Liquid Input

2- Gas Output

3- Gas temperature probe

4- Gas Mixture Input

5- O_2 Input

6- Stirrer Motor

7- Barometer

8- Flowmeter

9- Barometer

10- Gas Output

11- O_2 sensor

12- Regulation temperature

13- Pressure regulation pump

14- Liquid Temperature probe

15- Liquid Phase

16- Piston

17- Water from the pressure regulation pump

18- Basket containing reservoir rock and capillaries

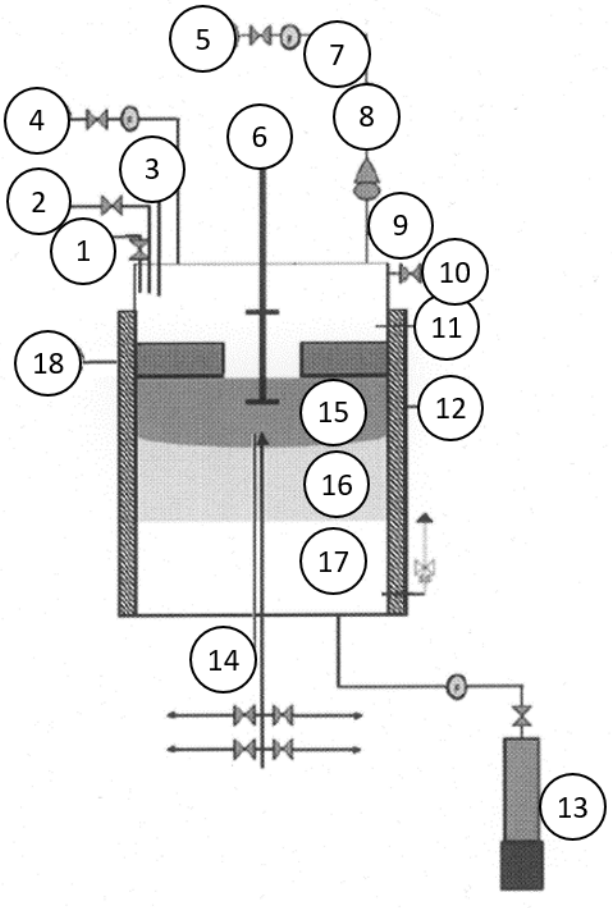

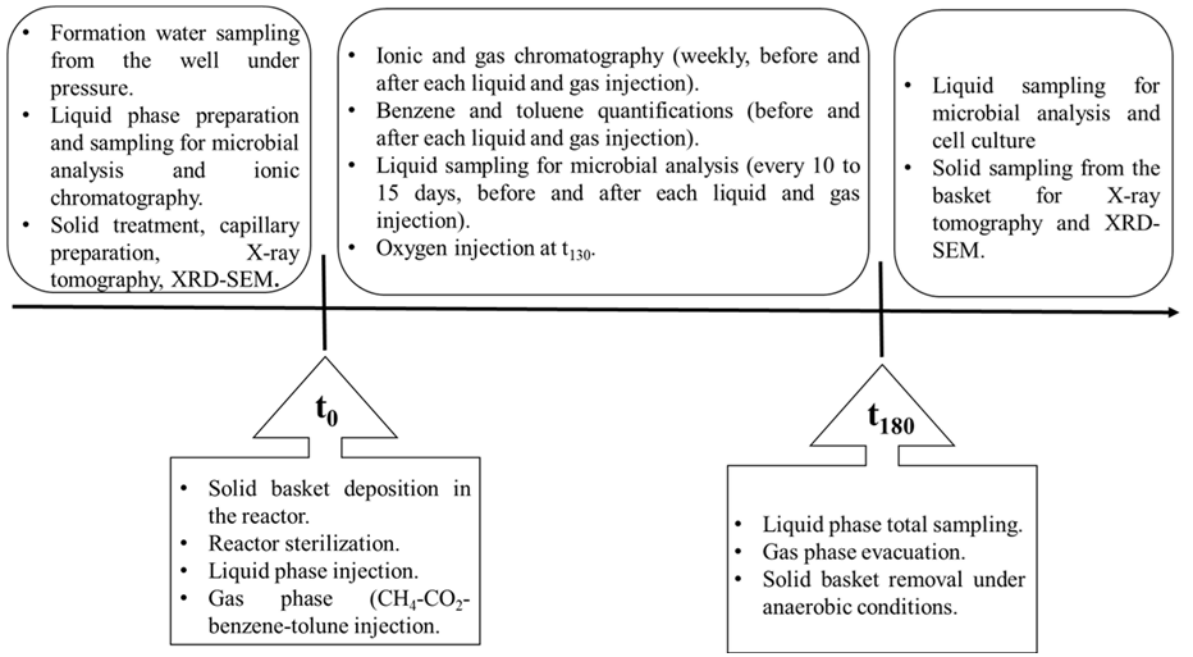
Formation water sampling from the well under pressure.
Liquid phase preparation and sampling for microbial analysis and ionic chromatography.
Solid treatment, capillary preparation, X-ray tomography, XRD-SEM.
Ionic and gas chromatography (weekly, before and after each liquid and gas injection).
Benzene and toluene quantifications (before and after each liquid and gas injection).
Liquid sampling for microbial analysis (every 10 to 15 days, before and after each liquid and gas injection).
Oxygen injection at t_{130}.
Liquid sampling for microbial analysis and cell culture
Solid sampling from the basket for X-ray tomography and XRD-SEM.
t_0
Solid basket deposition in the reactor.
Reactor sterilization.
Liquid phase injection.
Gas phase (CH_4-CO_2-benzene-tolune injection.
t_{180}
Liquid phase total sampling.
Gas phase evacuation.
Solid basket removal under anaerobic conditions.

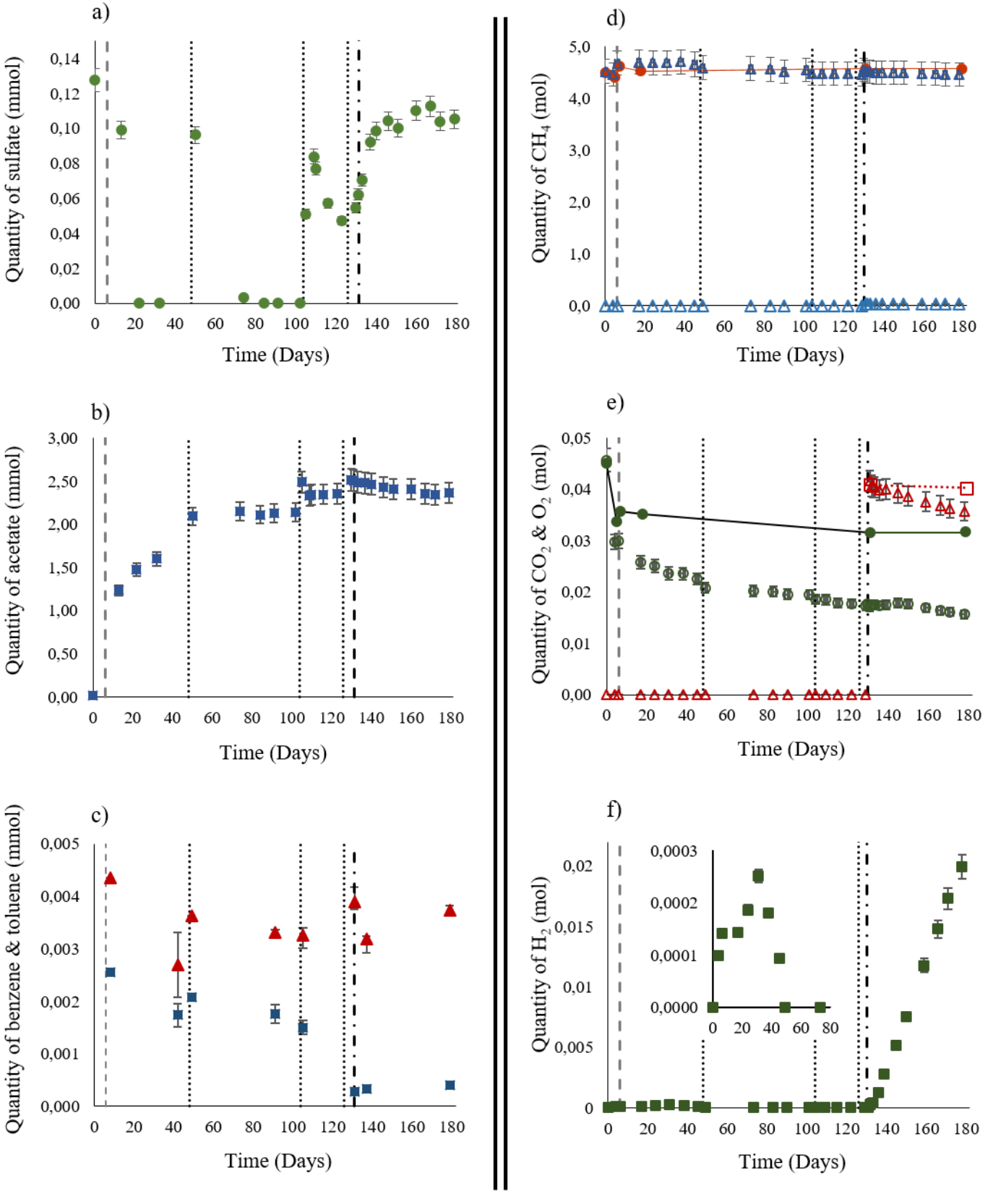
a)
Quantity of sulfate (mmol)
0,14
0,12
0,10
0,08
0,06
0,04
0,02
0,00
0 20 40 60 80 100 120 140 160 180
Time (Days)
b)
Quantity of acetate (mmol)
3,00
2,50
2,00
1,50
1,00
0,50
0,00
0 20 40 60 80 100 120 140 160 180
Time (Days)
c)
Quantity of benzene & toluene (mmol)
0,005
0,004
0,003
0,002
0,001
0,000
0 20 40 60 80 100 120 140 160 180
Time (Days)
d)
Quantity of CH_4 (mol)
5,0
4,0
3,0
2,0
1,0
0,0
0 20 40 60 80 100 120 140 160 180
Time (Days)
e)
Quantity of CO_2 & O_2 (mol)
0,05
0,04
0,03
0,02
0,01
0,00
0 20 40 60 80 100 120 140 160 180
Time (Days)
f)
Quantity of H_2 (mol)
0,02
0,015
0,01
0,005
0
0,0003
0,0002
0,0001
0,0000
0 20 40 60 80
0 20 40 60 80 100 120 140 160 180
Time (Days)

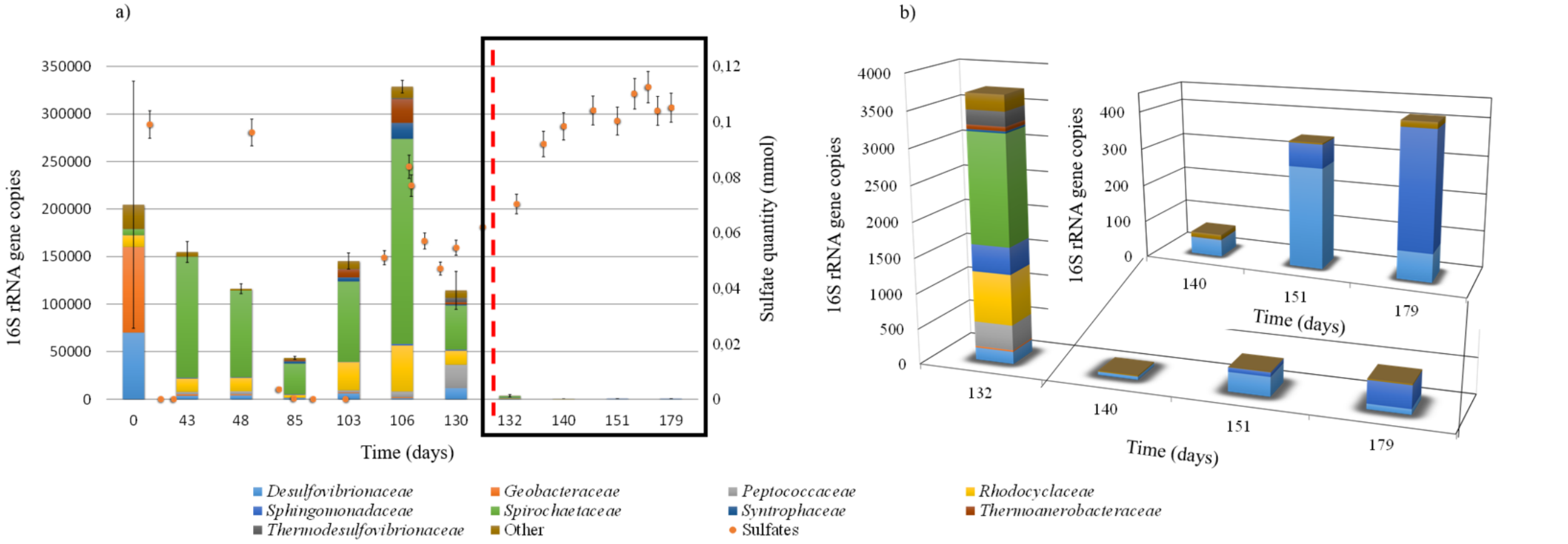
a)
16S rRNA gene copies
350000
300000
250000
200000
150000
100000
50000
0
0
43
48
85
103
106
130
132
140
151
179
Time (days)
0,12
0,1
0,08
0,06
0,04
0,02
0
Sulfate quantity (mmol)
b)
16S rRNA gene copies
4000
3500
3000
2500
2000
1500
1000
500
0
132
16S rRNA gene copies
400
300
200
100
0
140
151
179
Time (days)
140
151
179
Time (days)
Desulfovibrionaceae
Geobacteraceae
Peptococcaceae
Rhodocyclaceae
Sphingomonadaceae
Spirochaetaceae
Syntrophaceae
Thermoanerobacteraceae
Thermodesulfovibrionaceae
Other
Sulfates

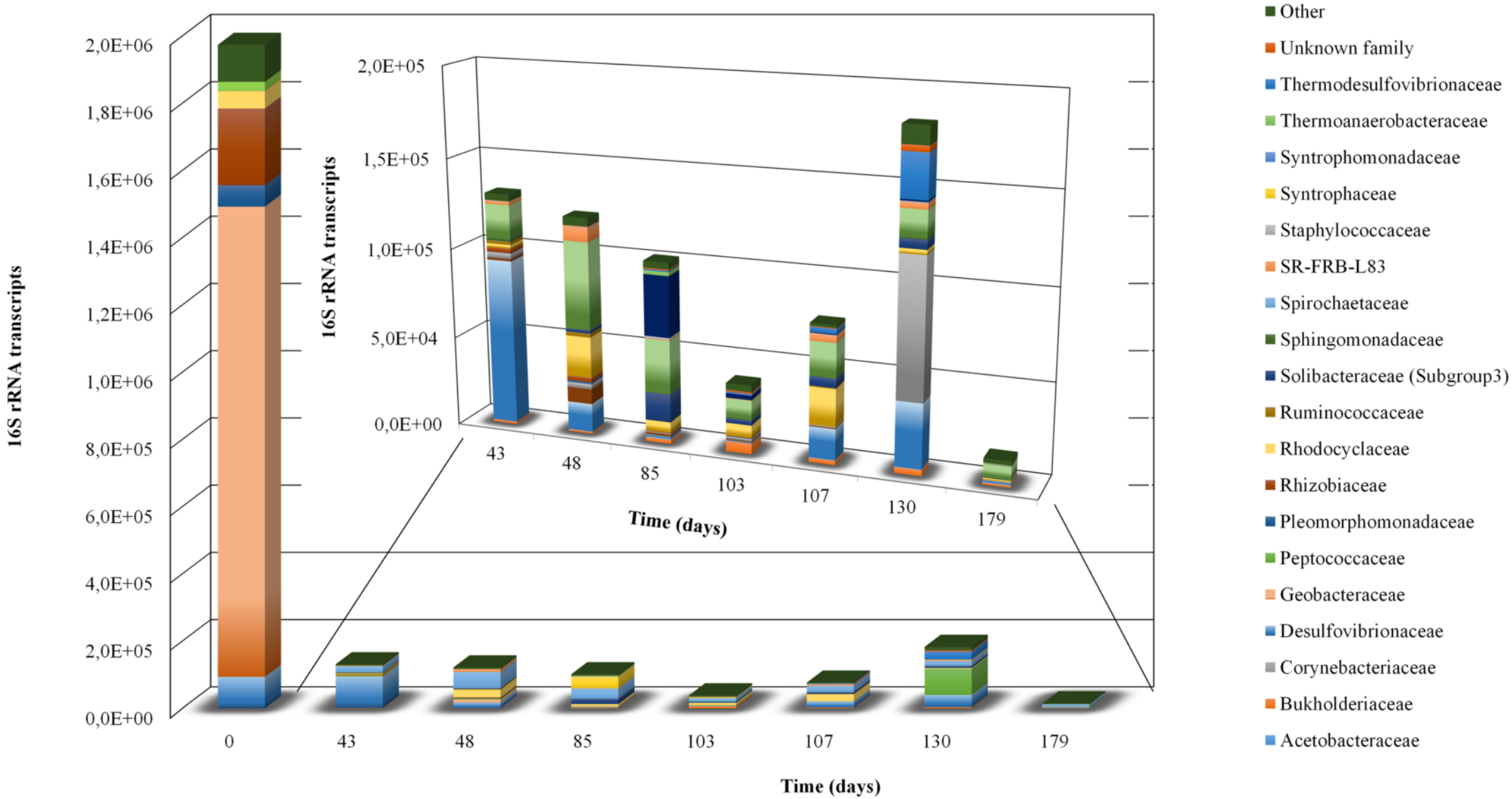
16S rRNA transcripts
2,0E+06
1,8E+06
1,6E+06
1,4E+06
1,2E+06
1,0E+06
8,0E+05
6,0E+05
4,0E+05
2,0E+05
0,0E+00
0
43
48
85
103
107
130
179
Time (days)
16S rRNA transcripts
2,0E+05
1,5E+05
1,0E+05
5,0E+04
0,0E+00
43
48
85
103
107
130
179
Time (days)
Other
Unknown family
Thermodesulfovibrionaceae
Thermoanaerobacteraceae
Syntrophomonadaceae
Syntrophaceae
Staphylococcaceae
SR-FRB-L83
Spirochaetaceae
Sphingomonadaceae
Solibacteraceae (Subgroup3)
Ruminococcaceae
Rhodocyclaceae
Rhizobiaceae
Pleomorphomonadaceae
Peptococcaceae
Geobacteraceae
Desulfovibrionaceae
Corynebacteriaceae
Bukholderiaceae
Acetobacteraceae

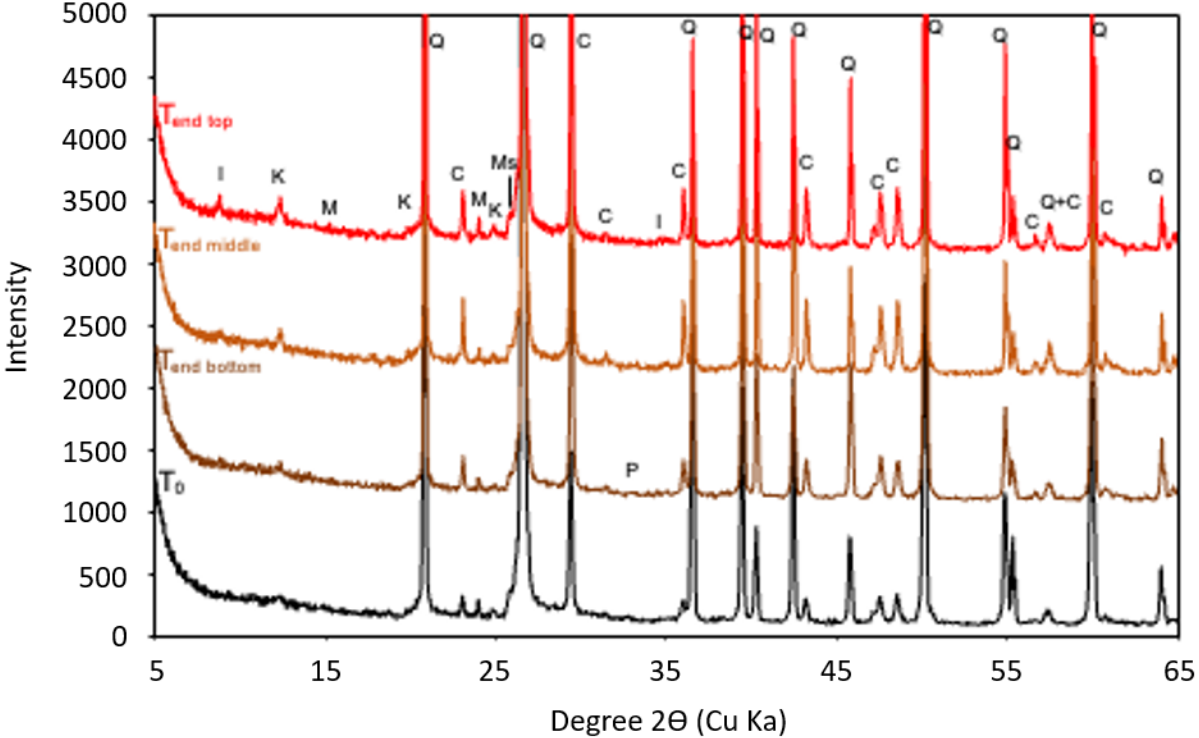
Intensity
5000
4500
4000
3500
3000
2500
2000
1500
1000
500
0
5
15
25
35
45
55
65
Degree 2Θ (Cu Ka)
T end top
T end middle
T end bottom
T0
I
K
M
K
C
M
K
Ms
Q
Q
C
C
I
C
Q
Q
Q
Q
C
Q
C
C
Q
Q
C
Q+C
C
Q
P

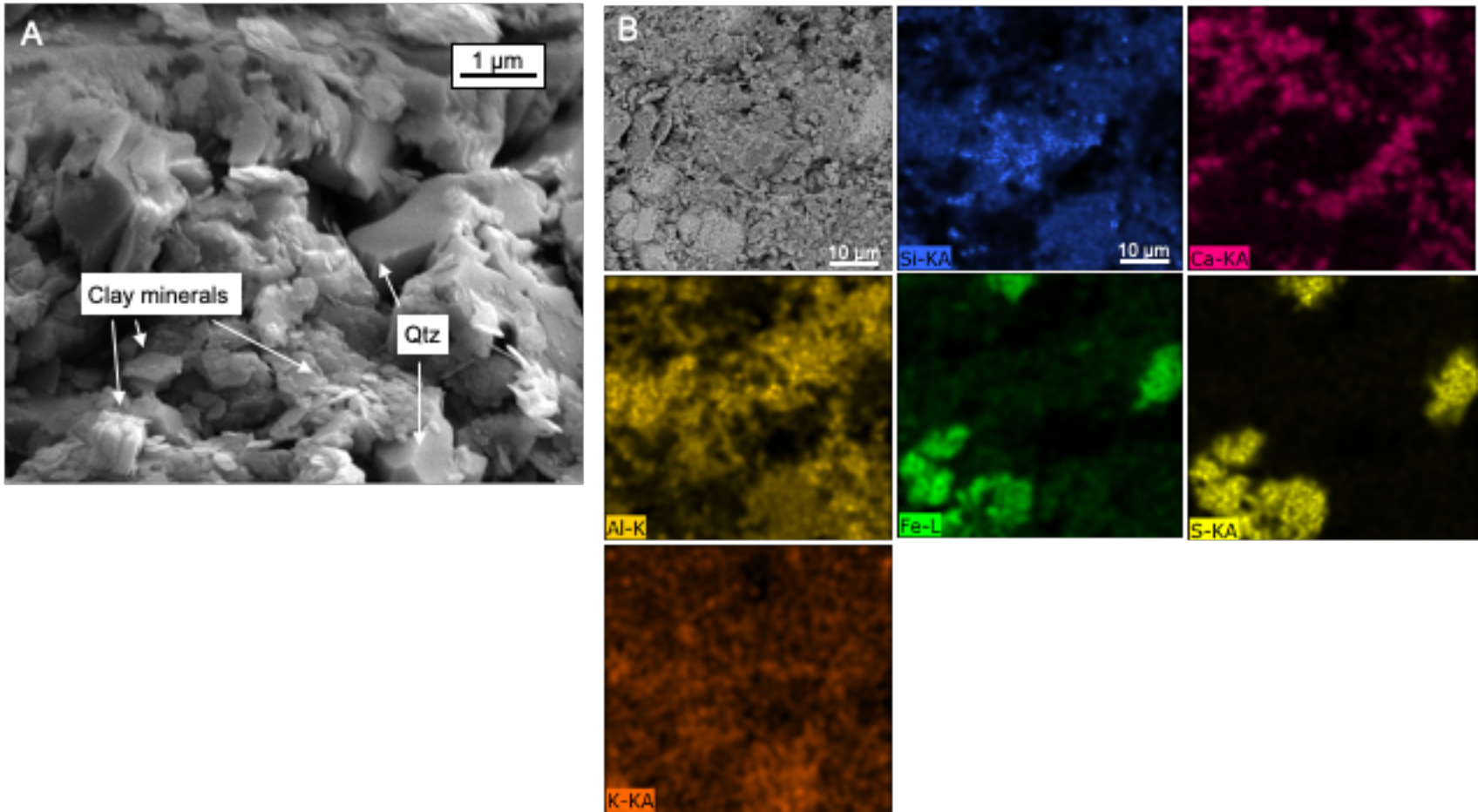
A
1 µm
Clay minerals
Qtz
B
10 µm
Si-KA
10 µm
Ca-KA
Al-K
Fe-L
S-KA
K-KA

Table 1 – Physico-chemical parameters and compounds of the formation water sampled from the deep aquifer (Ab_L_1 site), analyzed at atmospheric pressure.

Physico-chemical Parameters	Value	Unit
Pressure	60	Bar
Temperature	36	°C
pH	7.6	
Redox potential	-259	mV
Conductivity at 25 °C	330	µS_cm
Organic carbon	0.38	$mg.L^{-1}$
Compounds		
Chloride	0.2475	mM
Fluoride	0.0043	mM
Nitrate	0.0034	mM
Nitrite	0.0005	mM
Phosphate	0.0041	mM
Sulfate	0.0835	mM
Carbonate	0.0083	mM
Bicarbonate	3.0116	mM
Calcium	1.1884	mM
Iron	6.6122	µM
Dissolved iron	5.4486	µM
Magnesium	0.2465	mM
Potassium	0.1556	mM
Sodium	0.4930	mM

Table 2 – Standard deviation related to the 16S rRNA transcripts.

Time (Days)	Standard Deviation (16s rRNA transcripts)
0	1.14E+5
43	5.87E+5
48	5.32E+4
85	4.05E+3
103	2.01E+3
107	3.65E+3
130	6.19E+3
179	1.71E+3

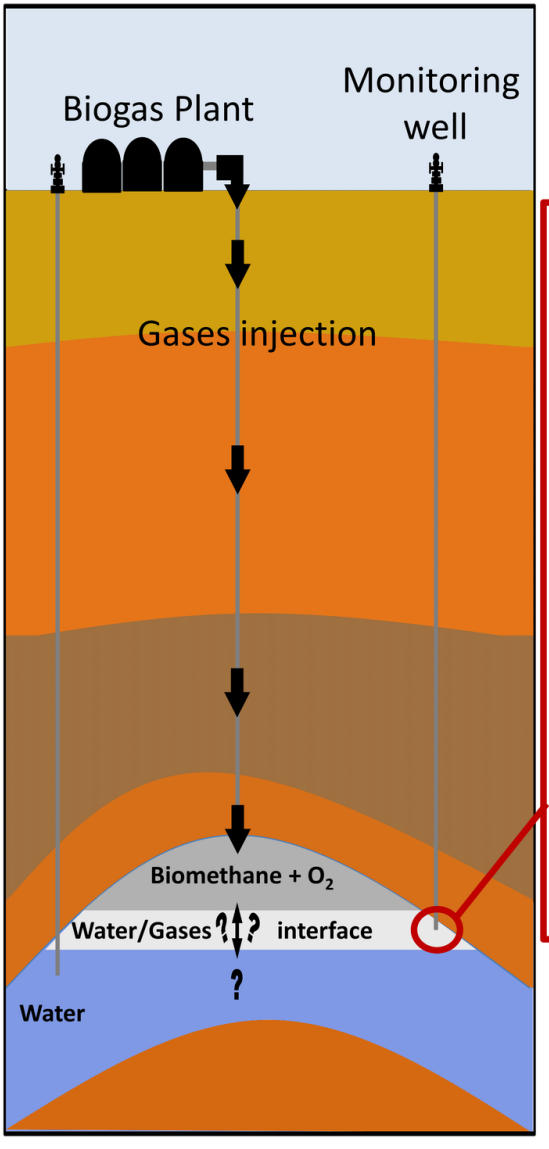

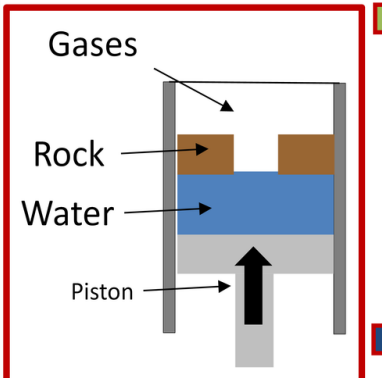

High Pressure reactor mimicking geological deep storage in aquifer conditions

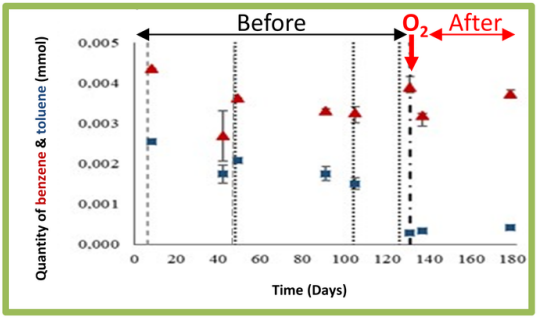

Physico-chemistry

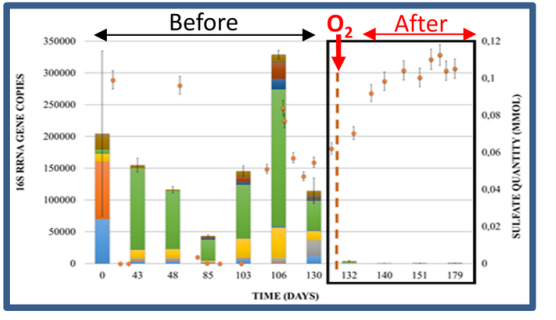

Microbiology

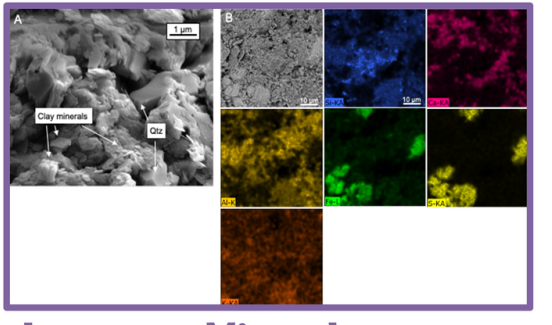

Imagery - Mineralogy